



Evolution of CDK1 Paralog Specializations in a Lineage With Fast Developing Planktonic Embryos

OPEN ACCESS

Edited by:

Kai Chen,
Kunming University of Science and
Technology, China

Reviewed by:

Takeshi Onuma,
Kagoshima University, Japan
Cristian Cañestro,
University of Barcelona, Spain
Alfonso Ferrández Roldán,
University of Barcelona, Spain
Andrew Swan,
University of Windsor, Canada

***Correspondence:**

Xiaofei Ma
Xiaofei.ma@uib.no
a530maxiaofei@163.com
Eric M. Thompson
Eric.Thompson@uib.no

†ORCID:

Xiaofei Ma
orcid.org/0000-0003-4826-9765
Eric M. Thompson
orcid.org/0000-0002-3756-9036

‡Present Address:

Xiaofei Ma,
College of Life Sciences, Northwest
Normal University, Lanzhou, China
Jan Inge Øvrebø,
Huntsman Cancer Institute, University
of Utah, Salt Lake City, UT,
United States

Specialty section:

This article was submitted to
Morphogenesis and Patterning,
a section of the journal
Frontiers in Cell and Developmental
Biology

Received: 05 September 2021

Accepted: 27 December 2021

Published: 28 January 2022

Citation:

Ma X, Øvrebø JI and Thompson EM
(2022) Evolution of CDK1 Paralog
Specializations in a Lineage With Fast
Developing Planktonic Embryos.
Front. Cell Dev. Biol. 9:770939.
doi: 10.3389/fcell.2021.770939

Xiaofei Ma^{1,2*†}, Jan Inge Øvrebø^{2,3‡} and Eric M. Thompson^{2,3*†}

¹College of Life Sciences, Northwest Normal University, Lanzhou, China, ²Sars International Centre, University of Bergen, Bergen, Norway, ³Department of Biological Sciences, University of Bergen, Bergen, Norway

The active site of the essential CDK1 kinase is generated by core structural elements, among which the PSTAIRE motif in the critical α C-helix, is universally conserved in the single CDK1 ortholog of all metazoans. We report serial *CDK1* duplications in the chordate, *Oikopleura*. Paralog diversifications in the PSTAIRE, activation loop substrate binding platform, ATP entrance site, hinge region, and main Cyclin binding interface, have undergone positive selection to subdivide ancestral CDK1 functions along the S-M phase cell cycle axis. Apparent coevolution of an exclusive CDK1d:Cyclin Ba/b pairing is required for oogenic meiosis and early embryogenesis, a period during which, unusually, CDK1d, rather than Cyclin Ba/b levels, oscillate, to drive very rapid cell cycles. Strikingly, the modified PSTAIRE of odCDK1d shows convergence over great evolutionary distance with plant CDKB, and in both cases, these variants exhibit increased specialization to M-phase.

Keywords: cyclin dependent kinase, determinant of specificity, nuclear envelope breakdown, PSTAIRE helix, tunicate, coenocyst, embryogenesis, gene duplication

INTRODUCTION

The complexity of the eukaryotic cell and its larger genome necessitates greater control over the organization of events during cellular division than for prokaryotic life. The eukaryotic protein kinase, CDK1, whose activity depends on unstable Cyclin regulatory subunits, has key roles in orderly triggering S and M phases from yeast to mammals (Santamaria et al., 2007), by sequential, regulatory phosphorylation of hundreds of substrate proteins. CDK activity levels progressively surpass response thresholds, to trigger serial events in S and M phases (Swaffer et al., 2016). Quantitative changes in CDK activity function as a coarse organizing mechanism for cell cycle transitions, with lower CDK activity resulting in higher affinity S-phase substrate phosphorylation, to carry out DNA replication, and higher activity driving mitotic entry *via* the phosphorylation of lower affinity mitotic substrates. CDK1 protein levels are constant during the cell cycle (Arooz et al., 2000), and are activated at each phase of the cell cycle by binding of stage-specific cyclins. The intrinsic activity of Cyclin-CDK1 complexes increases in correlation with the appearance of particular cyclins in the cell cycle (Ord and Loog 2019). G1/S cyclins generate CDK complexes with the lowest activity, which manifests in the lowest affinities (k_m) and the lowest catalytic activities (k_{cat}) toward substrates, whereas S-, G2-, and M-phase Cyclins form CDK complexes with higher affinities and catalytic

Abbreviations: CDK, cyclin dependent kinase; DoS, determinant of specificity; RNAi, RNA interference; NEBD, nuclear envelope breakdown.

activities towards substrates. The lower CDK activities generated by S- versus M-phase Cyclins also means that S-phase Cyclins do not achieve sufficient CDK1 activity levels to initiate mitosis, helping to ensure resolution of S- and M-phases. Compared to unicellular yeast, metazoans have also evolved CDK2, with lower intrinsic activity than CDK1 in the regulation of S-phase (Ord et al., 2019a). Although metazoan CDK1 has become more specialized to M-phase functions it still retains indispensable, ancestral, late S-phase functions (Katsuno et al., 2009; Farrell et al., 2012; Seller and O'Farrell, 2018; Szmyd et al., 2019).

In addition to modulating CDK activity, the Cyclins are also implicated in specifying CDK substrate targets. Cyclins bind different substrate docking motifs: RxF for S Cyclins and LxF for budding yeast M Cyclins, and these Cyclin docking pockets increase specificity to target subsets to further fine-tune the CDK threshold ladder (Koivomagi et al., 2011; Ord et al., 2019b). Most CDK substrates contain multiple target sites clustered in disordered regions (Holt et al., 2009), and phosphorylation cascades along these sites are shaped by precisely oriented docking interactions mediated by Cks1, the phospho-adaptor subunit of CDK1 (Koivomagi et al., 2011). Distances between phosphorylation sites and docking sites are critical for both Cyclin and Cks docking. The composition of phosphorylation sites with respect to serine versus threonine, and surrounding residues, combined with positioning of Cyclin and Cks docking motifs, creates a unique barcode on each substrate. The Cyclin-CDK-Cks1 complexes read the barcodes and assign execution of CDK-triggered switches to specified time points during the cell cycle (Ord et al., 2019a).

Canonical cell cycle regulation can be modified during development and growth. This is true of rapid mitotic cell cycles observed during early embryogenesis in a wide range of phyla and in the promotion of growth through endocycles in a number of organisms (Edgar and Orr-Weaver, 2001). Externally developing, nutrient-rich, non-feeding, embryos are at risk of predation, and rapid development is a means of mitigating this risk (Strathmann et al., 2002). Many marine planktonic larvae also continue fast development to first swimming in order to enhance survival (Staver and Strathmann 2002). The pelagic, tunicate, *Oikopleura dioica*, exhibits very rapid embryonic and larval development, undergoing metamorphosis to a feeding juvenile within 12 h at 15°C (Bouquet et al., 2009). Very rapid growth and extensive modulation of reproductive output over several orders of magnitude are then achieved through deployment of a variety of endoreduplicative cell cycle variants (Ganot and Thompson 2002; Ganot et al., 2007). These adaptations allow the organism to rapidly adjust population levels in response to algal blooms, during an extremely short chordate life cycle (6 days at 15°C). Accompanying this life history strategy is the deployment of a variety of cell cycle variants and considerable modification of the organism's molecular cell cycle regulatory complement (Campsteijn et al., 2012), including gene duplications to generate multiple CDK1 and Cyclin B paralogs.

All metazoans examined to date possess a single CDK1 ortholog that exhibits a highly conserved PSTAIRE motif in the critical α C-helix structural element located within the

N-lobe of CDK1 and CDK2. This element is an important interface in docking interactions with Cyclin partners and in contributing to formation of the kinase active site (Wood et al., 2019). *O. dioica*, aligns with other metazoans in possessing a CDK2 with a conserved PSTAIRE motif, but deviates distinctively in that it has evolved 5 CDK1 paralogs, all of which show deviations in the critical PSTAIRE motif (Campsteijn et al., 2012). Here, we have examined how these paralogs have arisen in the appendicularian lineage and to what extent they exhibit functional specializations along the CDK2-CDK1, S- to M-phase, cell cycle, regulatory axis. We show that the CDK1 substrate binding platform, activation loop, ATP entrance site, hinge region, and the main Cyclin binding interface, have all diversified under positive selection. In meiosis and early embryogenesis, CDK1 paralogs were sequentially activated across the cell cycle. Combinatorial knockdowns revealed collaboration of CDK2, CDK1a, CDK1b and CDK1d along the S- to M-phase axis in oogenic meiosis and early embryonic divisions. Interestingly, the Cyclin Ba and CDK1d paralog are located in proximity on the recently evolved *O. dioica* X chromosome, were co-expressed specifically during oogenic meiosis and early embryogenesis, and were required for these processes. Modifications of critical residues in the Cyclin B:CDK1 interface and the salt bridge, suggest that CDK1d and Cyclin Ba/b may have coevolved an exclusive interaction that does not interfere with the more canonical CDK1a/b/c:CycBc interactions in regulating M-phases during early developmental events. It is generally universal in metazoan mitotic cycles that CDK1 protein levels remain relatively constant throughout the cell cycle whereas Cyclin B levels oscillate and are up-regulated during M-phase. In contrast, we reveal a novel regulatory oscillation of levels of the CDK1d paralog, as opposed to its Cyclin Ba/b interacting partner, that drive early, very rapid embryonic cell cycles in this planktonic chordate.

RESULTS

Episodic Positive Selection of CDK1 Orthologs After Duplication

Metazoans possess a single CDK1, with the only known exception of *Oikopleura dioica*, where 5 CDK1 paralogs have been identified (Campsteijn et al., 2012). To trace the origins of this amplification we analyzed genomes and transcriptomes of five appendicularian species in the *Oikopleura* and *Fritillaria* genera (Naville et al., 2019). *CDK1a*, *b* and *c* were uniformly present, whereas *CDK1d* and *e* appear to have arisen from *CDK1c* specifically in *O. dioica*, the only known dioecious appendicularian (Figure 1A). Interspecies clustering of *CDK1* paralogs and interspecies conservation of their intron-exon structures (Supplementary Figure S1) suggest that *CDK1* amplification arose through early DNA-based duplication events in the *Oikopleura* lineage. Based on phylogenetic analyses, there was a first duplication that gave rise to *CDK1a* and a second paralog, which was further duplicated to give rise to *CDK1b* and *CDK1c*. *CDK1c* further gave rise to *O. dioica* specific *CDK1d* and *e*. *O. dioica* *CDK1c*, *d* and *e*

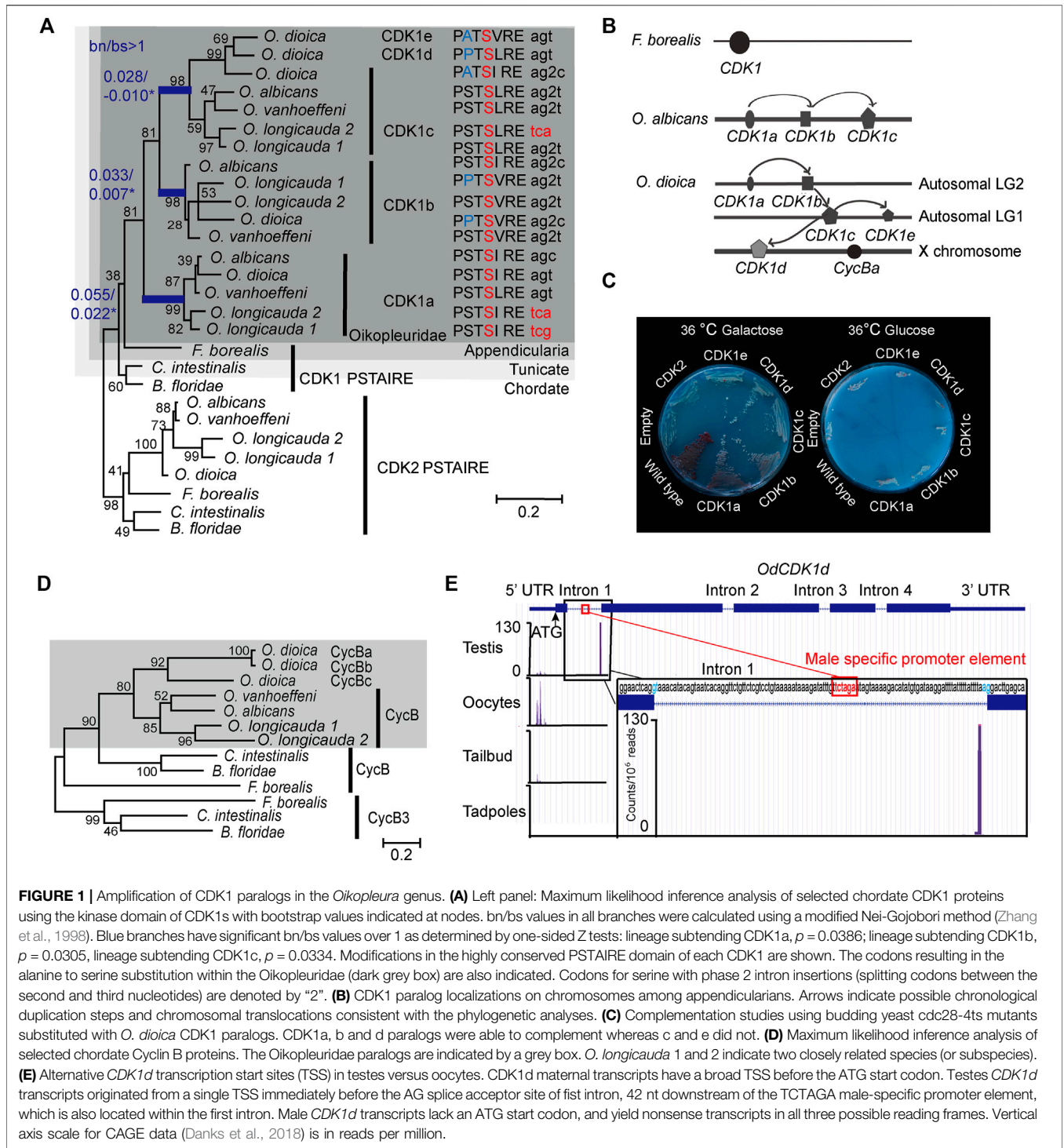


FIGURE 1 | Amplification of CDK1 paralogs in the *Oikopleura* genus. **(A)** Left panel: Maximum likelihood inference analysis of selected chordate CDK1 proteins using the kinase domain of CDK1s with bootstrap values indicated at nodes. bn/bs values in all branches were calculated using a modified Nei-Gojobori method (Zhang et al., 1998). Blue branches have significant bn/bs values over 1 as determined by one-sided Z tests: lineage subtending CDK1a, $p = 0.0386$; lineage subtending CDK1b, $p = 0.0305$, lineage subtending CDK1c, $p = 0.0334$. Modifications in the highly conserved PSTAIRE domain of each CDK1 are shown. The codons resulting in the alanine to serine substitution within the Oikopleuridae (dark grey box) are also indicated. Codons for serine for phase 2 intron insertions (splitting codons between the second and third nucleotides) are denoted by “2”. **(B)** CDK1 paralog localizations on chromosomes among appendicularians. Arrows indicate possible chronological duplication steps and chromosomal translocations consistent with the phylogenetic analyses. **(C)** Complementation studies using budding yeast *cdc28-4ts* mutants substituted with *O. dioica* CDK1 paralogs. CDK1a, b and d paralogs were able to complement whereas c and e did not. **(D)** Maximum likelihood inference analysis of selected chordate Cyclin B proteins. The Oikopleuridae paralogs are indicated by a grey box. *O. longicauda* 1 and 2 indicate two closely related species (or subspecies). **(E)** Alternative *CDK1d* transcription start sites (TSS) in testes versus oocytes. *CDK1d* maternal transcripts have a broad TSS before the ATG start codon. Testes *CDK1d* transcripts originated from a single TSS immediately before the AG splice acceptor site of first intron, 42 nt downstream of the TCTAGA male-specific promoter element, which is also located within the first intron. Male *CDK1d* transcripts lack an ATG start codon, and yield nonsense transcripts in all three possible reading frames. Vertical axis scale for CAGE data (Danks et al., 2018) is in reads per million.

are co-orthologs of *Oikopleura CDK1c*. The *O. dioica CDK1c*, *CDK1d* and *CDK1e* nomenclature in the literature could essentially be viewed as *CDK1ca*, *CDK1cb* and *CDK1cc*, respectively. To remain consistent with the existing literature we retain the c, d, and e nomenclature here. *O. albicans CDK1a*, b and c locate on the same chromosome. *O. dioica CDK1a* and b locate on the same autosome whereas *CDK1c* is present on a

different autosome that also contains *CDK1e* (Figure 1C). *CDK1d* is found on the X chromosome where, at a distance of 5 MB, the *cycBa* locus is also located. Following the classification system for paralog subtypes (Sonnhammer and Koonin 2002), *Oikopleura* genes in the *CDK1a* clade are orthologs, and *odCDK1a* and *b* are outparalogs to each other when comparing *O. dioica* with *O. albicans*, since CDK1 duplication happened before *O. dioica* and

O. albicans speciation. *O. dioica* CDK1c, d and e are inparalogs to each other when comparing *O. dioica* with *O. albicans*, since CDK1c duplication happened after *O. dioica* and *O. albicans* speciation.

Both the new Nei-Gojobori method (Zhang et al., 1998) and Codon-based models (Yang 2007) were applied to analysis of *Oikopleura* CDK1s. During the 2 rounds of gene duplication, the lineage subtending CDK1a (Figure 1A) experienced positive selection [bn/bs = 2.48, $P = 0.0386$, dN/dS(ω) = 41.01, $p = 0.081$, $P = 0.0481$], as did CDK1b [bn/bs = 4.72, $P = 0.0305$, dN/dS(ω) = 28.14, $p = 0.046$, $P = 0.003$] and CDK1c (bn/bs = infinite, $P = 0.033$, dN/dS(ω) = 999, $p = 0.066$, $P = 0.002$) (Figure 1A, Supplementary Table S1). To better understand positively selected sites identified by Codon-based models, we aligned CDK1 sequences from 15 metazoan phyla, and Cdc28 (an ortholog of metazoan CDK1) from budding yeast. Sites conserved in metazoan sequences, but substituted in *Oikopleura* CDK1 orthologs, were mapped to human CDK1 and CDK2 crystal structures (Supplementary Figures S2B, S3A). Determinants of kinase specificities (DoS) (Creixell et al., 2015) were aligned and the DoS that are conserved in metazoan CDK1 orthologs but substituted in *Oikopleura* CDK1 sequences were mapped to human CDK1-Cyclin B1 crystal structures (Supplementary Figure S3A). During kinase evolution, the critical catalytic residues, regulatory hydrophobic spine and catalytic hydrophobic spine have been conserved (Supplementary Figures S2A,B). The diversification of the substrate binding platform-activation segment, and indirect ATP binding sites, drive diversification of substrate specificity and substrate phosphorylation efficiency. *Oikopleura* CDK1s have the same active site as human CDK1 and yeast cdc28, including the Mg²⁺-binding loop (DFG), important residues in the catalytic loop, the catalytic hydrophobic spine, the regulatory hydrophobic spine and the salt bridge (Wood et al., 2019) (Supplementary Figure S2A). The bn/bs values below 1, observed among CDK1 paralog terminal branches, suggest that these paralogs are functional kinases under purifying selection. Conservation in the DFG+1 residues (Leu) in the 17 *Oikopleura* CDK1 sequences (Supplementary Figure S2A), suggests that they share with human CDK1, a preference for serine over threonine as a phosphor-acceptor residue in substrates (Chen et al., 2014). However, the ATP binding sites, substrate binding sites and Cyclin binding interfaces have diversified in *Oikopleura* CDK1 paralogs.

Substitutions in ATP Binding Sites

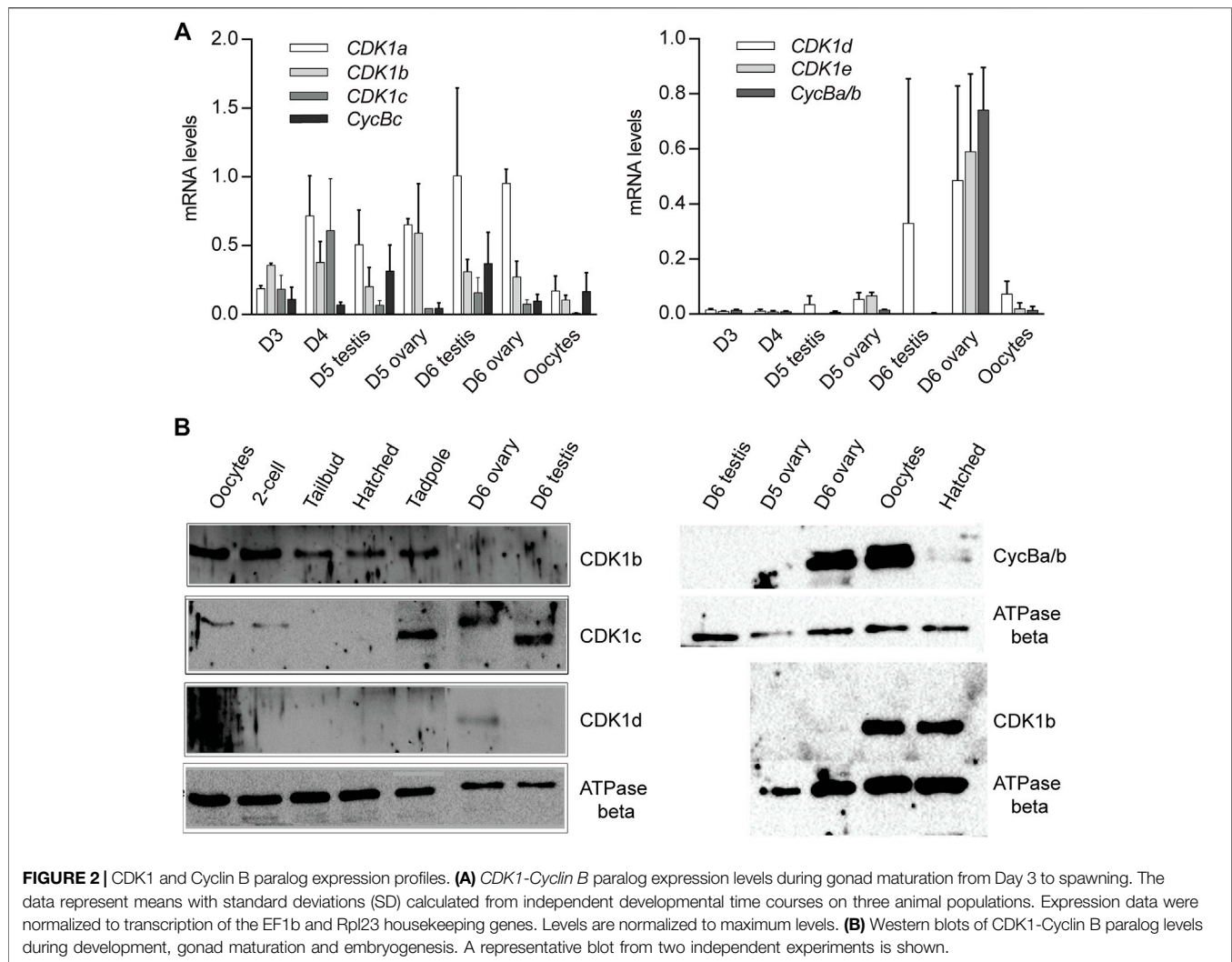
In the protein kinase family, the ATP binding site is very conserved, but adjacent areas not occupied by ATP are more variable, particularly in the hinge region and solvent accessible region (E81-K89, human CDK1 numbering) (Vulpetti and Bosotti, 2004). These sites modulate ATP affinity (Echalier et al., 2012). This region may determine the different catalytic efficiencies of CDK1 and CDK2, as substitutions in the hinge of CDK2, which mimic amino acids in this region of CDK1 (substitute N84, Q85 in CDK2 to 84S, 85M in CDK1), increase both ATP affinity (k_m ATP) and turn over (k_{cat}) (Echalier et al., 2012). In the opposite direction, a K89D/E

mutation in the CDK2 sequence, reduces k_{cat} . *Oikopleura* CDK1 paralogs have diversified in the hinge region and solvent accessible region. CDK1c paralogs exhibit an S84F/Y substitution whereas this site is conserved in CDK1a paralogs compared to the metazoan consensus (Supplementary Figures S2A,B). M85C substitution occurred in CDK1a of *O. vanhoeffeni*, *O. albicans* and *O. dioica*, after their divergence from *O. longicauda* (Supplementary Figure S2A). This substitution has been positively selected (Supplementary Table S1, Supplementary Figure S3A), possibly driving diversification of ATP affinity among CDK1 paralogs following their duplication. *Oikopleura* CDK1a and b orthologs have substitutions at K89, a residue that is conserved in CDK1 and CDK2 from yeast to metazoans (Supplementary Figures S2A,B). This raises the possibility that CDK1a and b may have lower ATP affinity and substrate phosphorylation efficiency compared to CDK1c, d and e paralogs. Indeed, as shown later, we found that CDK1d peaks in M phase whereas CDK1a was present earlier in interphase. The CDK1 L83 residue is also conserved from yeast to human, with the amide of L83 forming a hydrogen bond with the heteroaromatic adenine ring of ATP (Bao et al., 2011). This residue is conserved in CDK1a and c, but has been modified to L83M in the hinge region of all *Oikopleura* CDK1b orthologs (Supplementary Figures S2A,B). Thus, CDK1 paralogs have different signatures in their hinge regions and solvent accessible regions, suggesting diversification in their ATP affinities and catalytic efficiencies.

The conserved P61, is located in the N-lobe, in the loop connecting the PSTAIRE helix and β 4 of human CDK1 (Supplementary Figure S3A). Positive selection of a P61E substitution in all *Oikopleura* CDK1a orthologs (Supplementary Table S1) suggests that positive selection occurred after the initial CDK1 duplication but prior to speciation. This asymmetric adaptive evolution of an evolutionary conserved site in one of the duplicates, and conservation of this substitution within CDK1a orthologs, could be best explained by escape from adaptive conflicts after duplication (Des Marais and Rausher 2008).

Substitution in the Activation Segment

The activation segment forms an integral part of the substrate binding groove, and diversity in this loop contributes to the wide range of substrate specificities and affinities of protein kinases (Nolen et al., 2004). The structure of CDK1 suggests a mechanism through which activation loop flexibility, embedded in a more flexible CDK1 fold, allows CDK1 to accommodate a more diverse substrate set than CDK2 (Brown et al., 2015). These plastic properties may also contribute to its ability to partner non-cognate cyclins in the absence of other CDKs to drive a complete metazoan cell cycle. In *Oikopleura* CDK1 paralogs, sites in the activation segment that bind to substrate, P0 (L149, T166), P+1 (V164, V165) and P+3 (T161), are the same as in yeast and human CDK1 (Supplementary Figures S2A, S3B). However, several conserved sites in the activation segment have been dramatically modified in *Oikopleura* CDK1 paralogs, particularly in *O. dioica* CDK1c, d and e inparalogs. G154 is located at the tip of the human CDK1 activation segment



where it is important in forming the β turn in the short β hairpin structure when CDK1 binds to Cyclin B1 (Brown et al., 2015) (Supplementary Figure S3A). Human CDK2 cannot form this hairpin structure (Jeffrey et al., 1995), and this is a major difference in the activation segment between CDK1 and CDK2. The G154 site is conserved in yeast and metazoans, but has diversified in *Oikopleura* CDK1 paralogs. A G154N substitution occurred in *Oikopleura* CDK1a, G154S in *Oikopleura* CDK1b, and G154K in *O. dioica* CDK1c, d and e (Supplementary Figure S2A). This site is also identified as having experienced positive selection (Supplementary Table S1), suggesting adaptive diversification of the activation segment by disrupting the β -turn though substitution with large side chain residues. Immediately downstream of this substitution, *O. dioica* CDK1c, d and e all have an I157F substitution, whereas CDK1c paralogs from other *Oikopleura* species have an I157M substitution (Supplementary Figure S2A). *O. dioica* CDK1c, d and e also exhibit substitutions at the V159 and Y160 sites, two residues immediately upstream of the important, regulatory phospho T161 site (Supplementary

Figure S2A). The V159 site is also a DoS, conserved from yeast to humans (Supplementary Figures S2A, S3A). Finally, in human CDK1, L167 (conserved from yeast to human) is adjacent to the substrate P-2 residue (Brown et al., 1999; Bao et al., 2011) (Supplementary Figure S4). The L167M substitution found in all CDK1b and c orthologs, presents a larger side chain, which may affect affinity towards P-2 residues (Supplementary Figures S2A, S4).

Substitutions in the PSTAIRE Helix

The CDK1 PSTAIRE helix is invariant in metazoans and yeast. Mutation screens in yeast *cdc28* revealed that the exact PSTAIRE helix sequence (PSTAIREISLLKE) is required for cell division, and any mutations in this domain are lethal (Macneill and Nurse, 1993; Levine et al., 1999; Ahn et al., 2001). The A48V substitution in *cdc2* in *S. pombe* is dominant negative, as the mutant *cdc2* could bind Cyclin but could not be activated (Fleig et al., 1992), whereas an A48T substitution in *S. cerevisiae cdc28* inhibits CLB2 association (Ahn et al., 2001). Surprisingly, the PSTAIRE helix is modified in all *Oikopleura* CDK1 paralogs (Figure 1A) whereas

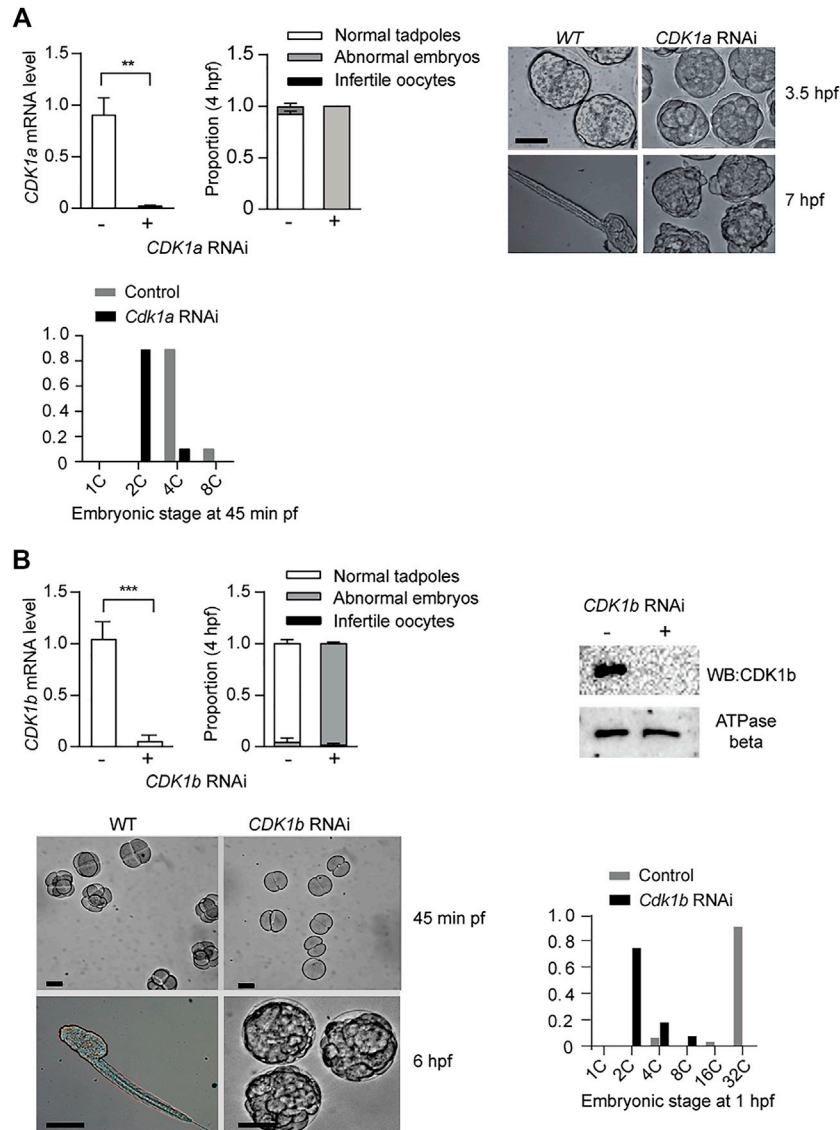


FIGURE 3 | *CDK1a*, *b*, and *d* knockdowns generate abnormal embryonic phenotypes. **(A)** *CDK1a* RNAi delays embryonic divisions and tadpoles fail to form. Upper left panel: efficient knockdown of *CDK1a* in oocytes spawned from ovaries injected with dsRNA against *odCDK1a* at D5. Upper Mid panel: When exposed to wild-type sperm, *CDK1a* deficient oocytes generated embryos that divided more slowly than wild-type and failed to hatch at 4 hpf (n1 = 3, n2 = 3). Upper right panel: images of delayed development in *CDK1a* deficient embryos. When wild-type embryos had developed to the late tailbud stage, *CDK1a* deficient embryos had only begun to gastrulate. At 7 hpf, tadpoles were observed in wild-type whereas *CDK1a* deficient embryos failed to reach the tailbud stage. The legend in **(A)** also applies to the respective panel in **(B)**. Bottom panel: distribution of developmental stages in *CDK1a* deficient and wild type embryos assessed at 45 min pf. Representative result of three independent experiment is shown. **(B)** Upper left panel: efficient knockdown *CDK1b* in oocytes spawned from ovaries injected with dsRNA against *odCDK1b* at D5 (n1 = 3, n2 = 4). Upper mid panel: When exposed to wild-type sperm, *CDK1b* deficient oocytes generated embryos that failed to hatch at 4 hpf (n1 = 3, n2 = 4). Upper right panel: Western blot showing absence of *CDK1b* protein in *CDK1b* RNAi embryos. Representative blot from three independent experiments is shown. Bottom left panel: *CDK1b* deficient embryos arrested before gastrulation (n1 = 3, n2 = 3). Bottom right panel: distribution of developmental stages in *CDK1b* deficient and wild type embryos assessed at 1 hpf. Representative result of three independent experiment is shown. **(C–E)**, Knockdown of *CDK1d* generated 3 different phenotypes at 1 hpf. **(C)** Left panel: efficient knockdown in oocytes spawned from ovaries that had been injected with dsRNA against *odCDK1d* at late D4 (C) (n1 = 3, n2 = 3). Right panel: abnormal division in all cases with a subset of embryos exhibiting more severe phenotypes of polar body extrusion but no cell division, or a complete lack of polar body extrusion and absence of any division (n1 = 3, n2 = 3). **(D)** Left panel: efficient knockdown in oocytes spawned from ovaries that had been injected with dsRNA against *odCDK1d* at early D5 (n1 = 3, n2 = 3). Right panel: proportion of embryonic phenotypes for *CDK1d* deficient embryos (n1 = 3, n2 = 3). **(E)** Left panel: efficient knockdown in oocytes spawned from ovaries that had been injected with dsRNA against *odCDK1d* at D5 (n1 = 3, n2 = 3). Right panel: proportion of embryonic phenotypes for *CDK1d* deficient embryos (n1 = 3, n2 = 3). The legend in **(E)** also applies to the respective panels in **(C)** and **(D)**. **(F)** Knockdown of *CDK1d* did not have any effect on the levels of Cyclin Ba/b, the Cyclin component of MPF in *O. dioica* oocytes (Feng and Thompson 2018). Representative blot from two independent experiments is shown. **(G)** Image comparisons of wild-type to *CDK1d* knockdown oocyte/embryo phenotypes 1 h post exposure to wild-type sperm. Left to right: WT cleavage stage embryos, infertile oocytes with no polar body extrusion, polar bodies extruded, but no division, and abnormally dividing embryos. Where indicated, data are mean (SD); ****p* < 0.001, ***p* < 0.01, **p* < 0.05. Scale bars: 50 μm.

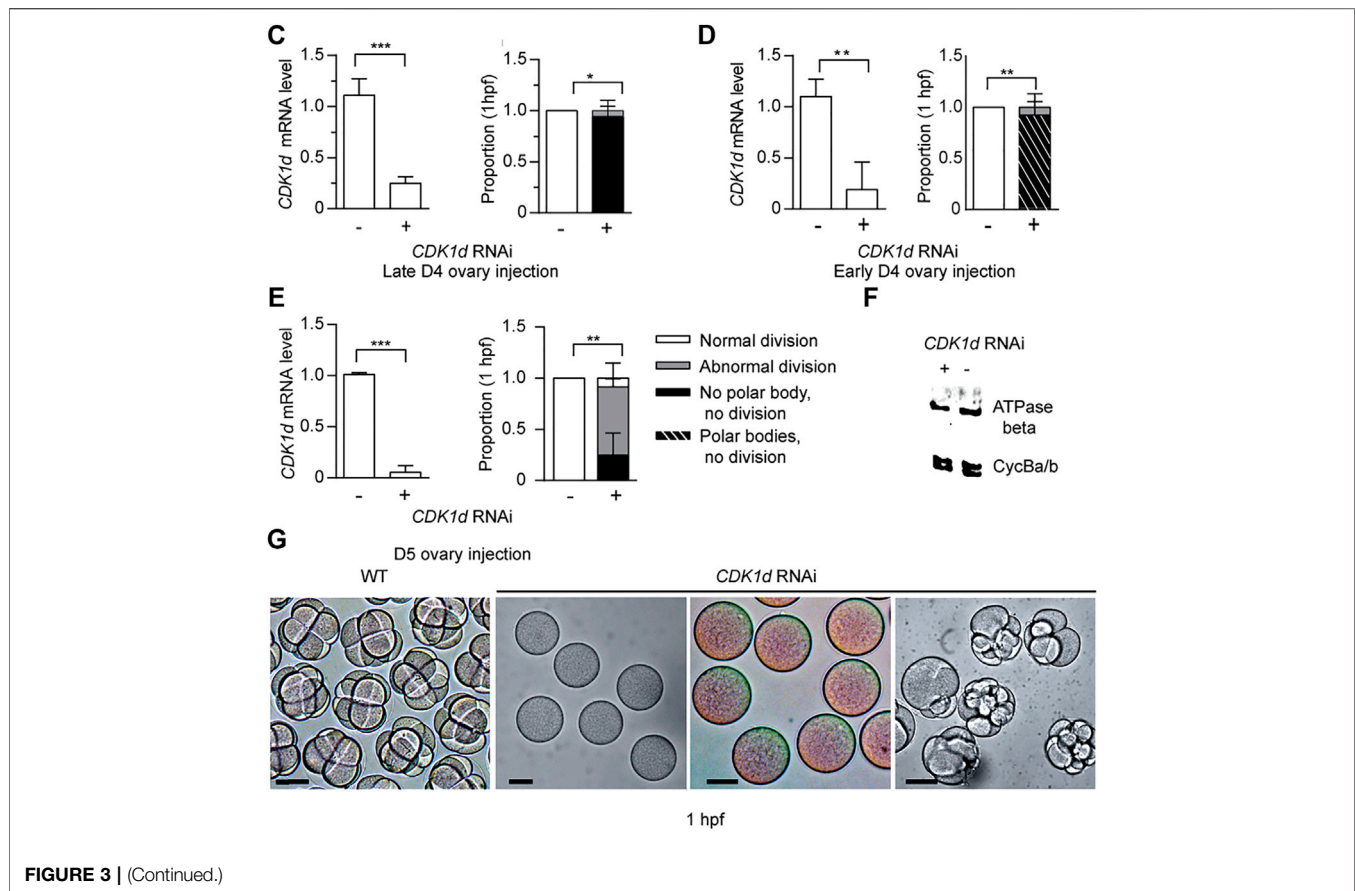


FIGURE 3 | (Continued.)

Oikopleura CDK2s retain the canonical PSTAIRE sequence. All of the 17 identified *Oikopleura* CDK1 sequences share the A48S substitution (Supplementary Figure S2A, Figure 1A). The S48 residues in *Oikopleura* CDK1 sequences are encoded by two disjoint codon sets, TCN and AGY, which cannot be interconverted by a single nucleotide mutation. Accordingly, switches between serine codons from the two sets can occur either directly, by simultaneous double (tandem) mutation (TC > AG), or indirectly, via two consecutive single-nucleotide substitutions (TC > AC > AG or TC > TG > AG). This is consistent with strong positive selection (Rogozin et al., 2016) at these sites in CDK1 sequences within the entire *Oikopleura* genus. Interestingly, coincident with the A48S substitution, codons for S48 in all CDK1b and c paralogs, except olCDK1c, have phase 2 intron insertions (Supplementary Figure S1, Figure 1A). This intron insertion is specific to *Oikopleura*, and is not found in any other metazoan CDK1.

O. dioica CDK1b and d (and *O. longicauda* CDK1b) have an additional S46P substitution in the PSTAIRE helix whereas *O. dioica* CDK1c and e have an S46A substitution at this residue (Figure 1A). The double proline predicts that the odCDK1b and d PSTAIRE helices would be shorter and exhibit an altered orientation compared to human CDK1. *O. dioica* CDK1a, b and d paralogs complemented yeast *cdc28* temperature sensitive mutants, whereas *O. dioica* CDK1c and e did not

(Figure 1C). *O. dioica* CDK1c, d and e inparalogs also share double S53C and L54T/S substitutions in the PSTAIRE helix (Supplementary Figure S2A). Human CDK1 S53 forms hydrogen bonds with Cyclin B1 L296 and G297 amide groups (Brown et al., 2015) (located at the C-terminal loop connected to the $\alpha 5$ helix) (Supplementary Figure S3C). Substituting serine at this site with cysteine may reduce CDK1c inparalog interaction interfaces with Cyclin B.

In summary, critical elements for catalysis are conserved in *Oikopleura* CDK1 paralogs, but they diverge in binding sites for ATP and substrates, suggesting qualitative differences in catalysis. Therefore, we set out to determine expression profiles and evaluate knockdowns of *O. dioica* CDK1 paralogs to characterize their individual functions in meiosis and early embryonic cell cycles.

Transcription of *CDK1d* and *Cyclin Ba/b* is Restricted to Oogenesis

CDK1a, b, c and *cycBc* are generally present in the *Oikopleura* genus (Figures 1A,D). In *O. dioica*, they were broadly expressed, in a sexually unbiased manner, in embryos, juveniles, and mature animals (Figure 2). As described in Campsteijn et al. (2012), Cyclins Ba and Bb are a recent duplication specific to *O. dioica* and share 97% amino acid identity. This makes it very difficult to

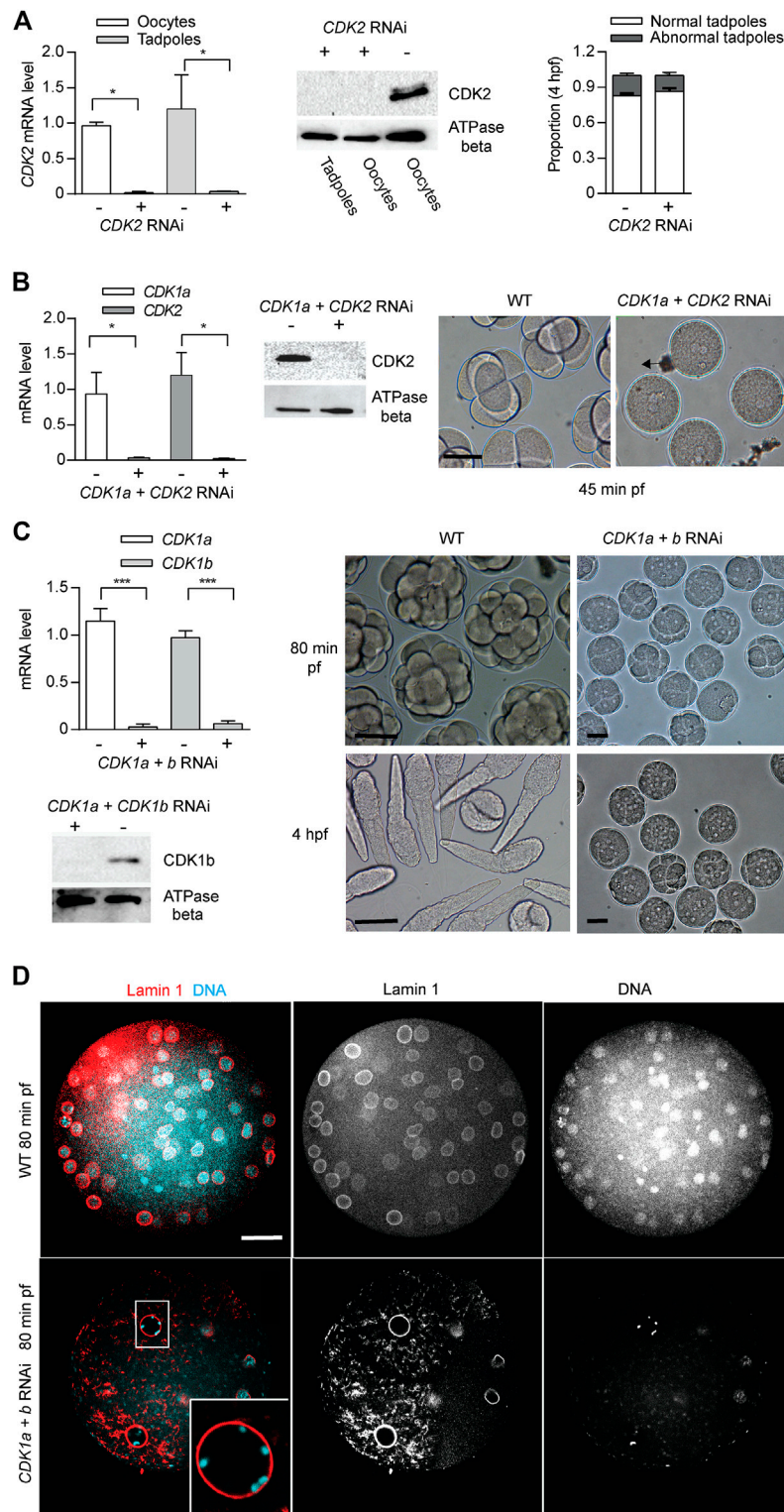


FIGURE 4 | CDK2 is dispensable for *Oikopleura dioica* embryogenesis. Synergistic defects of *CDK2* + *CDK1a* RNAi and *CDK2* + *CDK1b* RNAi in embryonic divisions. **(A)** *CDK2* is dispensable for embryonic divisions. Left panel: efficient knockdown of *CDK2* in oocytes and tadpoles, spawned from ovaries injected with dsRNA against *odCDK2* at D4 (n1 = 3, n2 = 3). Mid panel: Western blot showing absence of *CDK2* protein in *CDK2* RNAi oocytes and tadpoles. Representative blot from two independent experiments is shown. Right panel: no significant differences in developmental outcome between *CDK2* deficient and wild-type embryos (n1 = 3, n2 = 3). **(B)** Synergistic effect of *CDK2* + *CDK1a* RNAi on embryonic divisions. Left Panel: efficient knockdown of *CDK1a* and *CDK2* in oocytes from ovaries that had been *(Continued)*

FIGURE 4 | injected with dsRNA against *odCDK2* and *CDK1a* at D5 (n1 = 3, n2 = 3). Mid panel: Western blot showing absence of CDK2 protein in CDK1a + *CDK2* RNAi in oocytes. Representative blot from three independent experiments is shown. Right panel: at 45 min pf, *CDK1a* + *CDK2* deficient zygotes were arrested prior to pronuclear fusion. Scale bars: 50 μ m. **(C)** Synergistic effect of *CDK1a* + *b* RNAi on embryonic division. Upper left panel: efficient knockdown of *CDK1a* and *b* in oocytes from ovaries that had been injected with dsRNA against *CDK1a* + *b* at D5 (n1 = 3, n2 = 3). Lower left: Western blot showing absence of CDK1b protein in *CDK1a* + *b* RNAi oocytes. Representative blot from three independent experiments is shown. Right panel: *CDK1a* + *b* deficient zygotes finished 3 rounds of slowed divisions before arresting at the 4th–5th embryonic division. Scale bars: 50 μ m. Where indicated, date are mean (SD); ****p* < 0.001, ***p* < 0.01, **p* < 0.05. **(D)** Confocal images of Lamin 1 and DNA staining of wild-type versus *CDK1a* + *b* RNAi embryos at 80 min post-fertilization. *CDK1a* + *b* deficient zygotes arrest at prophase with super-condensed chromosomes at the nuclear periphery (inset) after the third division. Scale bars: 20 μ m.

distinguish Cyclin Ba from Bb when using antibody-based approaches. Therefore, as in Campsteijn et al. (2012), we use the combined Ba/b nomenclature here. In contrast, *CDK1d* and *e*, and *cycBa/b* were transcribed during oogenesis. Their transcripts persisted during early embryogenesis (Figures 2, 6A). *CycBa/b* was not expressed in juveniles or testes. Interestingly, CAGE data (Danks et al., 2015), revealed that *O. dioica* *CDK1d* has different transcription start sites (TSS) in testes and ovaries. The oocyte *CDK1d* TSS occurs before the ATG start codon located in the first exon. In testis, a sharp TSS located within the first intron yields nonsense transcripts (Figure 1E). Western blots confirmed that the CDK1d protein was present in ovaries but absent in testes (Figure 2B). *CDK1d* mRNAs began to drop after fertilization and dropped to very low levels at 2.5 h post-fertilization (Figure 6A). Given these differential expression patterns, we then undertook to knockdown the five CDK1 paralogs and 2 Cyclin Bs in *O. dioica* individually, or simultaneously, to explore functions of the expanded CDK1-Cyclin B complement.

CDK1a, b and d Collaborate in Embryonic Divisions: A Conserved PSTAIRE is not Required

The five *odCDK1* paralogs and *odCDK2* were each targeted for knockdown by RNAi. After injections of dsRNA in gonads of day 4 or 5 animals, oocytes were collected and processed to verify specific knockdown by RT-qPCR, and western blots. Successfully knocked down oocytes were exposed to wild type sperm and embryonic divisions were examined. Previous reports of *CDK1a* RNAi at day 4 demonstrated that this impaired vitellogenesis and meiosis resumption (Ovrebo et al., 2015; Feng and Thompson, 2018). *CDK1a* RNAi at day 5 avoided these defects and injected animals produced normal size oocytes. However, embryonic divisions were delayed and they failed to hatch (Figure 3A). When *CDK1b* was knocked down, embryonic cell cycles were also delayed and embryos arrested at gastrulation, corresponding to 2.5 h post-fertilization of normal embryos (Figure 3B). Knockdown of *CDK1d* yielded 3 phenotypes: a complete failure to emit polar bodies, arrest after polar body emission, or abnormal divisions after polar body emission (Figures 3C–G). These phenotypes reflect roles of *odCDK1d* in nuclear envelope breakdown (NEBD) (Ovrebo et al., 2015) and spindle assembly in meiosis I, for meiosis completion (Feng and Thompson, 2018), and subsequent mitotic divisions. No significant differences were observed in the proportions of normal hatching embryos between wild type, and any of the *CDK1c*, *e*, or *c+e* RNAi knockdown embryos (Supplementary Figure S5). *CDK1c* and *e* have very

similar PSTAIRE helices (PATSIVRE, Figure 1A), they failed to rescue yeast *cdc28* mutants, and they were also dispensable for embryonic divisions.

CDK2 is dispensable for early mouse early embryogenesis and mitotic cycles in cultured vertebrate cells (Santamaria et al., 2007). Consistent with these observations, *odCDK2* RNAi embryos divided normally and hatched with correct timing (Figure 4A). CDK2 is the only CDK in *Oikopleura* that has a canonical PSTAIRE helix. This indicates that the exact sequence in the conserved metazoan CDK1, PSTAIRE helix, is not required for *Oikopleura* embryonic divisions. After emission of polar bodies, *CDK1a* + *CDK2* RNAi zygotes arrested prior to pronuclear fusion (Figure 4B). The synergistic defects during the cell cycle caused by *CDK1a*+*CDK2* RNAi suggests CDK1 and CDK2 have overlapping roles in interphase. Since *CDK2* RNAi embryos divided normally, defects arising from *CDK1a*+*CDK2* RNAi suggest *CDK1a* could complement CDK2's roles in interphase during embryonic divisions. Immunostaining of tadpoles developed from oocytes injected with *CDK1a*-GFP capped mRNA, showed CDK1a located to the nucleus during interphase (Supplementary Figure S6). *CDK1a+b* RNAi embryos arrested at the 4th or 5th division at prophase with super-condensed chromosomes closely juxtaposed to the nuclear lamina (Figures 4C,D). The synergistic defects during the cell cycle cause by *CDK1a+b* RNAi suggests collaborative roles of *CDK1a* and *CDK1b* during prophase, the point at which *CDK1b* localized to nucleus (Supplementary Figure S6).

Coevolution of *Oikopleura dioica* CDK1d and Cyclin Ba/b

Vertebrate Cyclin B1 is required for meiosis and mitosis. Most invertebrates, except *C. elegans* (van der Voet et al., 2009), have a single ortholog of vertebrate Cyclin B1/B2 (Figure 1D), and this ortholog is required for meiosis and mitosis (Okano-Uchida et al., 1998). Oscillation of Cyclin B levels orchestrate CDK1 kinase activity during M-phase. As for other invertebrates, all 4 hermaphroditic *Oikopleura* species have a single Cyclin B, whereas dioecious *O. dioica* has Cyclins Ba and Bb in addition to Cyclin Bc. The *cycBa* gene is located on the X chromosome, and is specifically expressed in ovaries. Knockdown of Cyclin Bc, showed no significant differences in Cyclin Ba/b levels, H1 kinase activity in oocytes, or embryonic development compared to wild type (Figure 5A), indicating that Cyclin Bc is dispensable for meiosis and embryonic divisions. In contrast, *cycBa/b* RNAi oocytes were defective for embryonic division (Figure 5B). We previously revealed the role of Cyclin Ba/b in GVBD and spindle

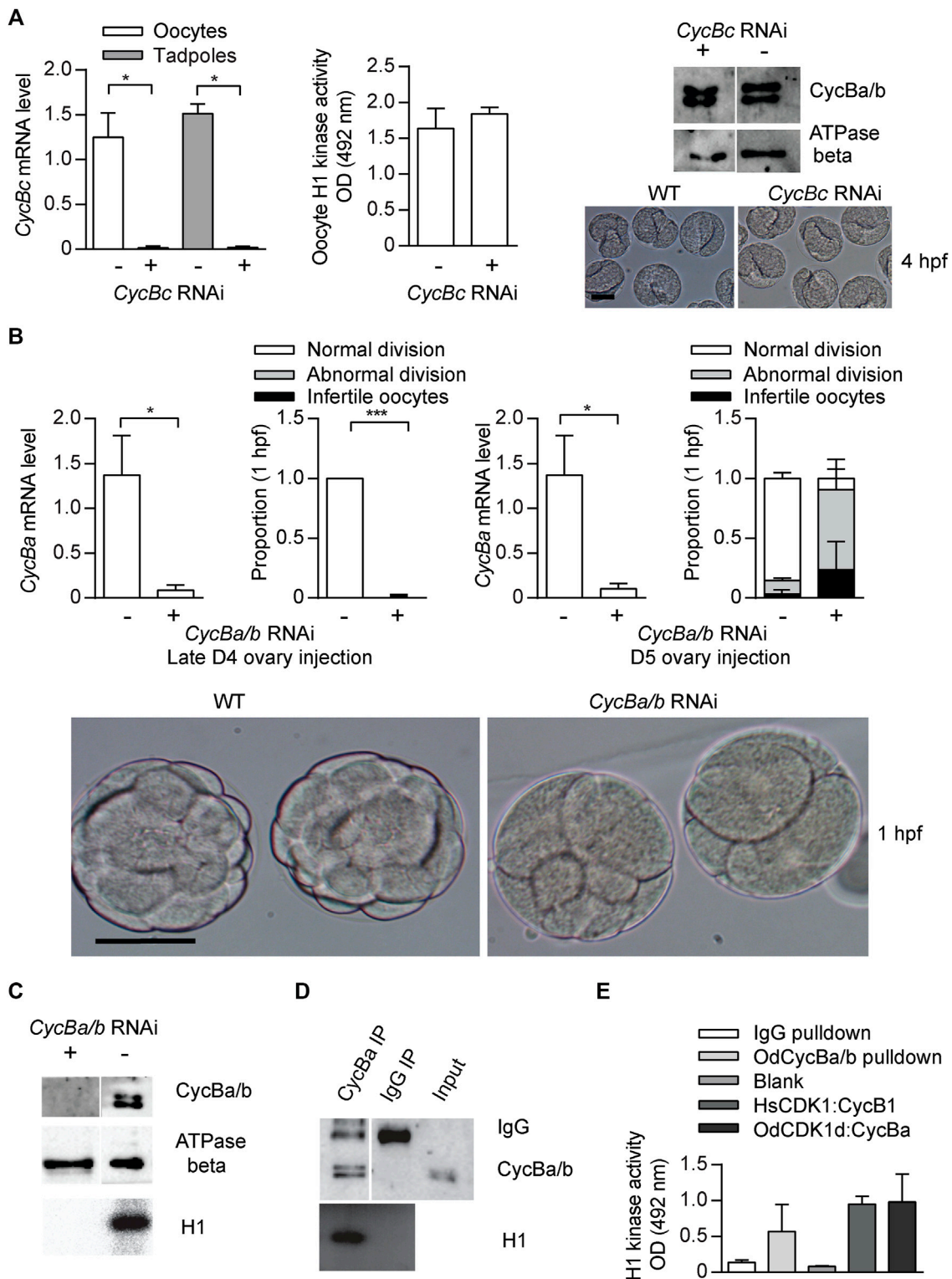


FIGURE 5 | Cyclin Ba/b, is required for *O. dioica* embryonic cell cycles, whereas Cyclin Bc is dispensable. **(A)** Cyclin Bc is dispensable for embryonic divisions. Left panel: efficient knockdown *cycBc* in oocytes (n1 = 3, n2 = 3) and tadpoles (n1 = 2, n2 = 3) spawned from ovaries that had been injected with dsRNA against *cycBc* at D5. Mid panel: no significant difference in mean H1 kinase activity between *cycBc* deficient and wild-type oocytes (metaphase I arrested, n1 = 3, n2 = 3). Upper right panel: Western blot showing that knockdown of *cycBc* had no effect on protein levels of Cyclin Ba/b. Representative blot from three independent experiments is shown. Lower right panel: images show Cyclin Bc deficient and wild-type embryos had identical phenotypes at the tailbud stage, 4 hpf. **(B)** Knockdown of *cycBa/b* generated 2 (Continued)

FIGURE 5 | different phenotypes at 1 hpf. Upper 1st panel: efficient knockdown of *cycBa/b* in oocytes spawned from ovaries that had been injected with dsRNA against *cycBa/b* at late D4 (n1 = 3, n2 = 3). Upper 2nd panel: Cyclin Ba/b deficient oocytes exposed to wild type sperm generated two embryonic phenotypes: infertile and abnormal divisions. Data represent the proportion of phenotypes in 50 zygotes derived from each ovary (n1 = 3, n2 = 3). Upper 3rd panel: efficient knockdown of *cycBa/b* in oocytes spawned from ovaries that had been injected with dsRNA against *cycBa/b* at D5 (n1 = 3, n2 = 3). Upper 4th panel: proportion of embryonic phenotypes for Cyclin Ba/b deficient oocytes spawned from ovaries that had been injected with dsRNA against *cycBa/b* at D5. Where indicated, data are mean (SD); *** $p < 0.001$, ** $p < 0.01$, * $p < 0.05$. Bottom panel: images show abnormal division phenotypes, compared to wild-type at 1 hpf. Scale bars: 50 μm . **(C–E)** CycBa/b-CDK1d complexes have histone H1 kinase activity. **(C)** H1 kinase activity was present in wild type oocytes but absent in *cycBa/b* RNAi knockdown oocytes (Feng and Thompson, 2018). **(D)** Cyclin Ba/b immunoprecipitates from oocytes had H1 kinase activity whereas IgG oocyte immunoprecipitates did not. Representative result from three independent experiments is shown. **(E)** H1 kinase activity levels of *O. dioica* Cyclin Ba/b pulldowns compared to IgG pulldowns and *in vitro* expressed complexes of Human (Hs) CDK1:Cyclin B1 and *O. dioica* (Od) CDK1d:Cyclin Ba. The data represent mean (SD) of three independent experiment.

assembly in meiosis (Feng and Thompson, 2018). Therefore, in *O. dioica* oogenic meiosis and early embryonic cleavage cycles, Cyclin Ba/b was required, whereas Cyclin Bc was dispensable.

Among the oikopleurids, CDK1d and Cyclin Ba specifically appear in *O. dioica* and share several features: X chromosome location, ovary-specific expression, similar degradation dynamics after fertilization (**Figures 6A,B**) and similar RNAi phenotypes in meiosis and mitosis. Therefore, we wished to determine if they form an active kinase complex. Cyclin Ba/b immunoprecipitates possessed H1 kinase activity, whereas lysates from infertile *cycBa/b* RNAi oocytes lose H1 kinase activity (**Figures 5C,D**). This led us to test whether *in vitro* constituted odCDK1d-Cyclin Ba complexes possesses kinase activity. GST-odCDK1d recombinants expressed in insect sf9 cells were insoluble. Co-expression with his-Cyclin Ba improved GST-odCDK1d solubility. Purified GST-odCDK1d:his-Cyclin Ba complexes possessed H1 kinase activity (**Figure 5E**). Surprisingly, the conserved Cyclin B Y170 residue which is critical for CDK1 binding is divergent in odCyclin Ba/b (replaced by His), whereas it is conserved in odCyclin Bc (**Supplementary Figures S7A,B**). A Y170A substitution is known to completely abolish CDK1: Cyclin B interaction in mouse, human, *Xenopus laevis* and *Ciona intestinalis* (Goda et al., 2001; Bentley et al., 2007; Levasseur et al., 2013; Levasseur et al., 2019). The CDK1d:Cyclin Ba/b complex also has modified residues at the position of the salt bridge (Goda et al., 2001) (**Supplementary Figures S7A,B**), which is in spatial proximity to Y170. This suggests that CDK1d and Cyclin Ba/b may have coevolved an exclusive interaction that does not interfere with the more canonical CDK1a/b/c:CycBc interactions.

Oscillation of CDK1 Levels, Instead of Cyclin B Levels, Orchestrates Early Embryonic Divisions

In marine invertebrates and in *Xenopus* embryos, mitosis is driven by accumulation of Cyclin B to a threshold required to activate CDK1, and mitotic degradation of Cyclin B inactivates CDK1, allowing mitotic exit. Cyclin Ba/b was stocked in *O. dioica* oocytes and was progressively degraded during early embryogenesis, dropping to low levels by 2.5 hpf (**Figure 6B**). CDK1d also reached low levels during this same period (**Figure 6A**). We then performed higher resolution sampling of Cyclin Ba/b levels at 2 min intervals during the first embryonic cell cycle. Morphologies of the zygotes were recorded at each time point and samples were divided into 2 aliquots and assayed for Cyclin Ba/b protein levels and H1 kinase activity. Consistent with

cell cycle progression, H1 kinase activity oscillated, peaking 20 min post-fertilization, when the nuclear envelope had disappeared and spindles were visible (**Figure 6F**). H1 kinase levels dropped at 23 min post fertilization, when cleavage furrows formed and dropped to a basal level at 28 min post fertilization, when abscission occurred, and two nuclei were visible. Surprisingly, CDK1d levels oscillated during the first cell cycle, in contrast to CDK1b and c levels which remained constant (**Figures 6C,D,F,G**). CDK1d levels and H1 kinase activity peaked together at 20 min post fertilization, when NEBD occurred and the spindle assembled. CDK1d levels then peaked again, coincident with a rise in H1 kinase activity during the second cell cycle (**Figures 6E–G**). Contrary to the oscillation of CDK1d levels, Cyclin Ba/b levels did not oscillate during the first 2 embryonic cycles (**Figures 6F,G**), instead, dropping at later embryonic stages. This latter observation is similar to *Drosophila* preblastoderm cycles, where neither bulk levels of Cyclin B, nor the bulk activity of CDK1 kinase oscillate, with progressive depletion of maternally stocked Cyclin B only leading to oscillations in Cyclin B levels at later developmental stages (Edgar et al., 1994). A key, and novel difference in *O. dioica* is that CDK1d levels did oscillate during these first embryonic cycles.

DISCUSSION

Oikopleura dioica exhibits high intrinsic rates of natural population increase (r) (0.68 d⁻¹ to 1.07 d⁻¹), well above the normal range for a metazoan of its size (Troedsson et al., 2002). The parameter, r , is increased by decreasing generation time, and/or by increasing egg number. In *O. dioica*, generation time is highly heritable and genetically correlated with r , whereas fecundity is much less heritable and not genetically correlated with r (Lobon et al., 2011). This emphasizes the importance of generation time in setting *O. dioica* fitness and is evidence of a life-history trait that has been strongly constrained by evolution (Deibel and Lowen 2012). The short duration of embryogenesis can be a direct target for selection to increase r .

We propose a working model for *O. dioica* cell cycle regulation under the framework of multiple CDK1 paralogs during oogenesis and rapid, early embryogenesis (**Figure 7**). Individual, or combined, knockdowns of CDK1c and e, did not generate any detectable phenotypes. Of note, neither of these CDK1 paralogs was able to complement yeast *cdc28* mutants. Similar to observations in mouse embryos and cultured vertebrate cells, CDK2, the only CDK with a

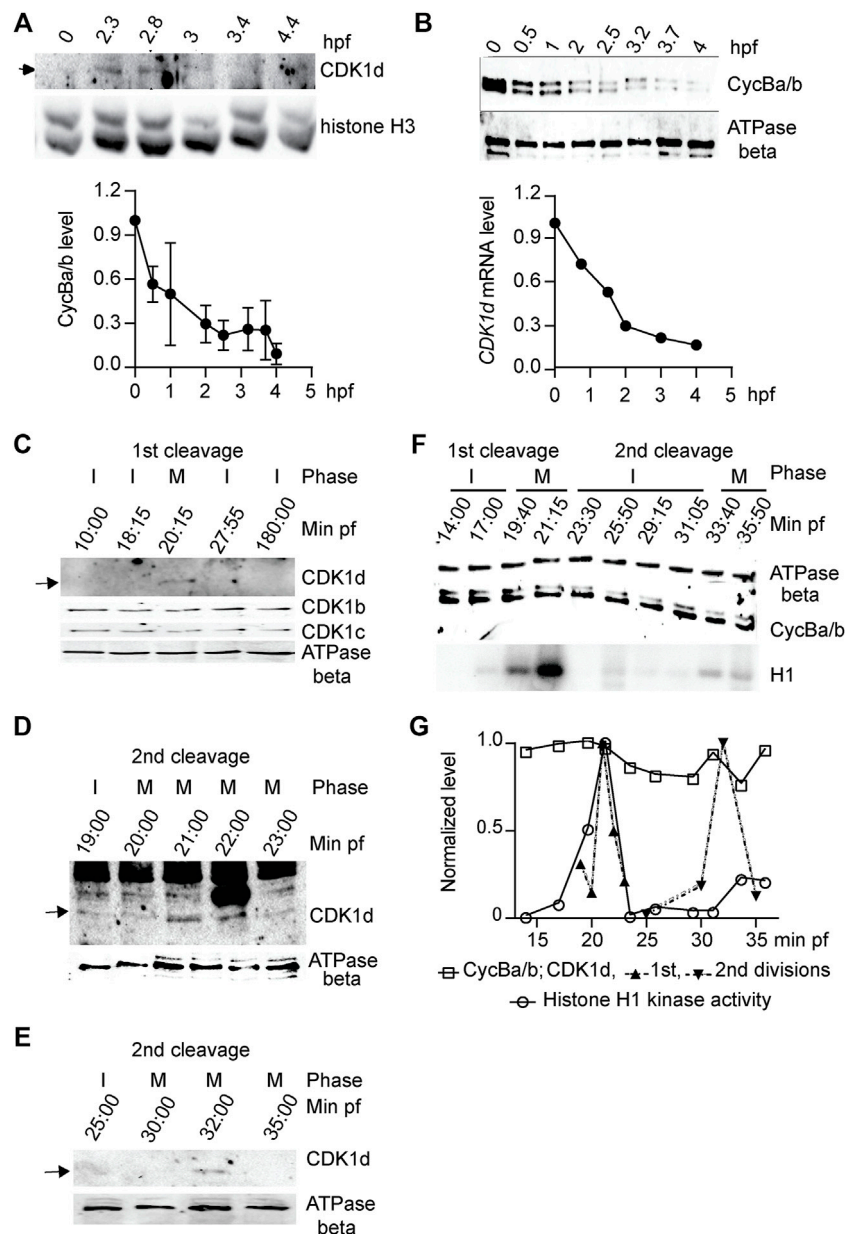
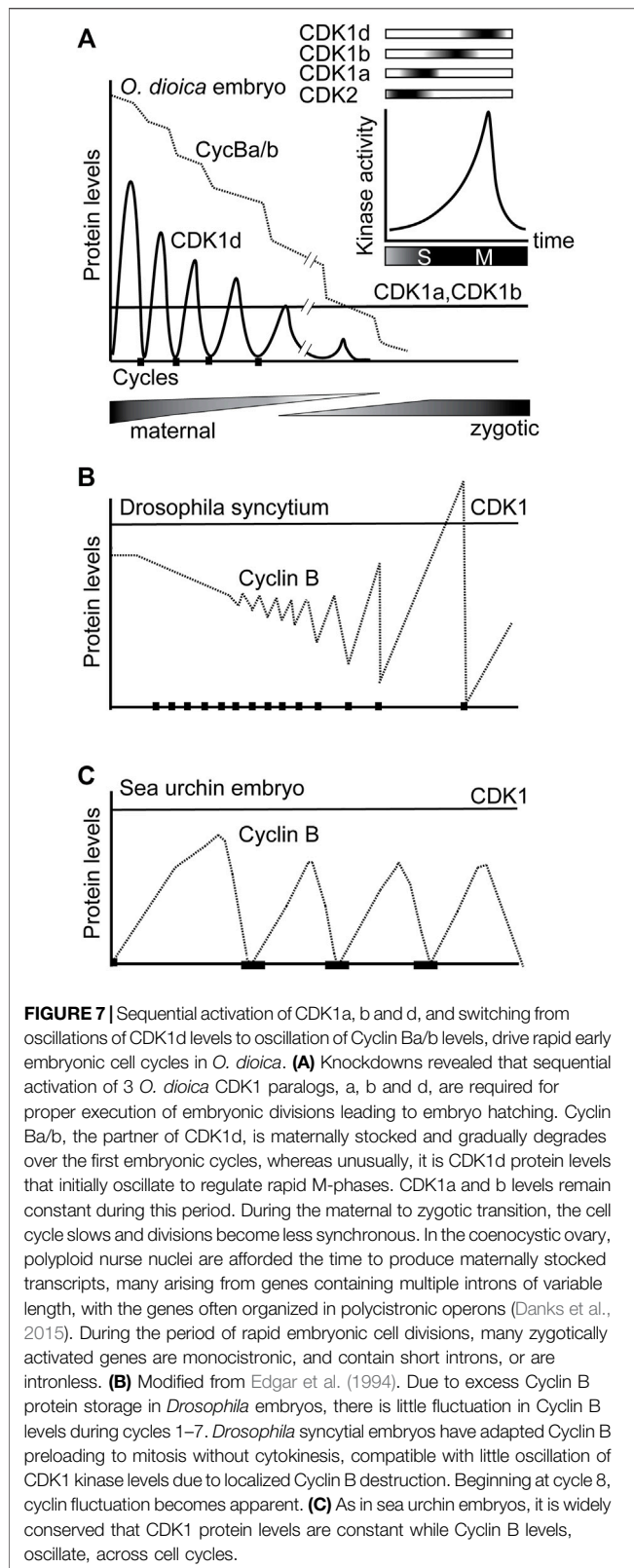


FIGURE 6 | CDK1d levels oscillate during early embryonic cell cycles. **(A)** Upper panel: Western blot of CDK1d levels during the first 4 h of development with histone H3 as a loading control. Lower panel: *CDK1d* mRNA levels were quantified during early embryonic development by qRT-PCR, normalized to levels in unfertilized oocytes. **(B)** Cyclin Ba/b levels do not oscillate but instead, decline steadily during early embryogenesis. Upper panel: Western blot of Cyclin Ba/b during the first 4 h of development with ATPase beta as a loading control. Lower panel: quantification of Cyclin Ba/b levels, normalized to levels in unfertilized oocytes. The data represent mean (SD) of three independent experiments. **(C–E)** CDK1d levels peaked in M phase of first two mitotic embryonic cell cycles. **(C)** Western blot of CDK1b, c, and d levels during the first 3 hpf. Arrow indicates the CDK1d band. I, interphase; M, M-phase. **(D)** Sampling of CDK1d levels at 1-min intervals around M phase of the first embryonic cell cycle. Arrow indicates the oscillation of the CDK1d band. **(E)** Sampling of CDK1d levels around M-phase of the second division cycle. Arrow indicates the oscillation of the CDK1d band. **(F)** Western blot analyses of Cyclin Ba/b levels and histone H1 kinase activity during the first two embryonic cell cycles. Cyclin Ba/b levels remained elevated, whereas H1 kinase activity oscillated, with peaks in the first two M-phases. Representative result from three independent experiments is shown. **(G)** Quantification of Cyclin Ba/b, CDK1d and H1 kinase activity during the first two embryonic cell cycles.

canonical PSTAIRE helix in *Oikopleura*, was dispensable for completion of meiosis and early embryonic divisions, as *CDK2* RNAi zygotes divided and hatched normally (Figure 4A). On the other hand, normal early embryonic divisions required 3 CDK1 paralogs (Figures 4, 5, 7, Supplementary Figure S5), none of

which contain a canonical PSTAIRE helix (Figure 1A). Depletion of CDK1a or b alone, delayed embryonic divisions (Figures 3A,B), whereas depletion of CDK1d abolished meiotic NEBD (Ovrebø et al., 2015), disrupted meiosis completion and caused abnormal embryonic cell cycles (Figures 3C–G). Knockdown



of CDK1d also depleted oocytes of histone H1kinase activity (Feng and Thompson 2018), as did knockdown of its binding partner, Cyclin Ba/b (Figure 5C). Double knockdowns of CDK2

and CDK1a arrested zygotes at the pronuclear stage (Figure 4B) whereas double knockdowns of CDK1a and b generated multinucleate embryos with irregular cell division patterns that failed to hatch (Figures 4C,D). CDK1d had critical functions in completion of meiotic M-phases and early embryonic divisions, during which it showed an unusual oscillation of protein levels that peaked in M-phase and decreased during interphase. CDK1d protein dynamics correlated well with the peak of H1 kinase activity and spindle formation during M phase (Figures 6C–H).

The 3 CDK1 paralogs are sequentially activated in a tiling pattern when embryos traverse late S- to M-phase, suggesting a further subdivision of CDK1 tasks and substrate targeting, beyond the CDK1-CDK2 subdivision that occurred much earlier in metazoan evolution. An additional, interesting feature of the *O. dioica* CDK1 paralog complement, is that it is CDK1d protein levels rather than its partner, Cyclin Ba/b, the only essential Cyclin B for *O. dioica* oogenic meiosis and early embryonic cell cycles, which oscillates during early embryonic cell cycles (Figures 6C–H). This contrasts the generally universal oscillation of Cyclin B levels on a background of stable CDK1 protein levels characteristic of metazoan cell cycle regulation.

During the maternal to zygotic transition, initial, rapid cell cycles, followed by progressive slowing, are a widespread occurrence in a number of species, indicating a consistent benefit to this strategy throughout the evolution of animals with externally deposited eggs (Farrell and O'Farrell, 2014; Yuan et al., 2016). This strategy converges on modulating the activity of the cell cycle driver, CDK1: weak inhibitory phosphorylation of CDK1 drives rapid cycles without gap phases, and when inhibitory phosphorylation is introduced, catalyzed by Wee and Myt1 kinases, the cell cycle slows and gap phases are inserted (Tsai et al., 2014). *O. dioica* and, the arthropod model, *Drosophila*, are characterized by a number of similarities with respect to oogenesis and early embryogenesis. Both utilize a syncytial strategy during oogenesis (albeit with significant differences in details), where polyploid nurse nuclei generate transcripts that code for materials stocked in the oocytes, which house largely transcriptionally quiescent meiotic nuclei. Both generate excess Cyclin B protein storage in oocytes, with progressive Cyclin B destruction during succeeding embryonic cycles. They diverge, however, in adaptations of rapid mitotic cycles to Cyclin B preloading. *Drosophila* syncytial embryos adapt Cyclin B preloading to mitosis without cytokinesis, compatible with little oscillation of CDK1 kinase levels due to localized Cyclin B destruction (Edgar et al., 1994; Huang and Ruff 1999). In contrast, completion of cytokinesis during the rapid mitoses of *O. dioica* embryonic cycles appears to require oscillation of CDK1 kinase levels (Figures 6F,G). CDK1d oscillations may be an adaptation to the coenocystic ovary structure and Cyclin Ba/b preloading. Another possible benefit to storage of Cyclin Ba/b, rather than CDK1d, could be that progressive destruction of Cyclin Ba/b by the anaphase promoting complex during embryogenesis would deplete

Cyclin Ba/b, facilitating switching of key cell cycle regulators after hatching. In this regard, regulators, such as CDC25, Wee1, and Emi2, critical in controlling important embryonic cell cycle transitions in other organisms (Farrell and O'Farrell, 2014; Tsai et al., 2014; Yuan et al., 2016), are all duplicated in the *O. dioica* genome (Danks et al., 2013).

Coenocystic oogenesis is a common feature of the Oikopleuridae (Ganot et al., 2006), allowing synchronous oocyte growth and maturation as an adaptation to a semelparous, opportunistic life style. The oikopleurid lineage also shares the presence of CDK1a, b and c paralogs. This raises questions as to the relationship between the specific gain of the CDK1d-Cyclin Ba/b complex in *O. dioica*, their linkage on the recently evolved X chromosome, and their ovary-specific expression. This pattern could be explained by resolution of sexual antagonism by gene duplication (Connallon and Clark 2011) and higher linkage disequilibrium on the X chromosome (Schaffner 2004). For genes that function both in hermaphrodite ovary and testes, the coenocystic ovary structure evokes conflict between different transcriptional regulation of those genes in polyploid nurse nuclei in the ovary, versus diploid germline progenitor cells in the testis. CDK1c does not show sexually biased gene expression (Figure 2A) (Campsteijn et al., 2012). CDK1c duplication giving rise to CDK1d and e in *O. dioica* may have mitigated sexual antagonistic conflict by allowing CDK1d (sexually biased expression to ovaries) to evolve essential ovarian functions. The X chromosome location of CDK1d might facilitate CDK1d ovary-specific expression since duplicates beneficial to females preferentially accumulate on the X chromosome where they are exposed to selection twice as often in females versus males (Connallon and Clark 2011). Indeed, when compared to zygotic promoters, maternal promoters in *O. dioica* are located on the X-chromosome more frequently than expected, ($\chi^2 = 43.34$, $df = 1$, $p = 4.61 \times 10^{-11}$), revealing a female-bias of X-linked genes in *O. dioica* (Danks et al., 2018). X-linkage of *CDK1d* and *cycBa* loci would then efficiently sustain linkage disequilibrium, reinforced through selection on the recently formed X chromosome (Bachtrog et al., 2009). Since there will be no recombination in the heterogametic male, this would contribute to an increase in sweeping to fixation in the population.

In *O. dioica*, the 3 CDK1 paralogs (a, b and d), which are required for correction execution of early embryonic cell cycles, exhibit sequence diversification on their activation segments, ATP binding sites and Cyclin B interaction interfaces. This raises the possibility of different k_{cat}/k_m catalytic outputs or phosphorylation site specificities during these rapid cell cycles. With respect to the K89 residue in the hinge region, both CDK1a and b, which participate in events preceding CDK1d, share a K89E/D substitution. This substitution would likely reduce CDK1 k_{cat} . CDK1a, b and d also have non-overlapping activation segments, suggesting CDK1 paralogs may have different affinities toward the same substrate phosphorylation site and/or different phosphorylation site

preferences. The sequential activation of CDK1a, b and d may provide a more stepwise, as opposed to progressive, increase of kinase activity, which may enhance and sharpen transitions towards early, middle and late substrates across early embryonic cell cycles. In metazoan cell cycles, the division of labor between CDK1 and CDK2 is not absolute. CDK1 retains essential roles in late S phase that CDK2 does not efficiently complement (Katsuno et al., 2009; Nakanishi et al., 2010; Farrell et al., 2012). Inactivation of CDK1 in temperature-sensitive CDK1 mutant cell lines (FT210) resulted in a prolonged S phase accompanied by ineffective firing of late replicon clusters and reduced the density of active origins during late S phase (Katsuno et al., 2009). In *Drosophila* pre-mild blastula transition S phases, it is CDK1 activity, rather than CDK2 activity that regulates late replication (Farrell et al., 2012; Seller and O'Farrell, 2018). The requirement for CDK1 in late S phase, coexists with its need to be repressed during early S phase (Larochelle et al., 2007) and its control in late S phase by Chk1 (Lemmens et al., 2018), to prevent premature triggering of M phase (Szmyd et al., 2019). In *O. dioica*, the conflict of CDK1's roles in the metazoan cell cycle of regulating both late S and M phase, might be relaxed by CDK1 duplication and subsequent partitioning of ancestral CDK1's roles in S and M phase to specific paralogs. Our results indicate that CDK1a collaborates with CDK2 to drive S phase and suggest that this paralog may exhibit reduced risk of triggering M phase, through lower intrinsic kinase activity, arising from substitution in hinge region and solvent accessible region (Supplementary Figure S2). On the other hand, the CDK1d paralog has become a specialist of M phase events without additional constraints imposed by regulation of late DNA replication. This may reflect adaptation to very rapid embryonic cell divisions in this planktonic organism.

A conformation change of the very highly conserved PSTAIRE helix is central to CDK1 inactivation/activation transitions (Huang et al., 2012). It is therefore surprising that this sequence was modified in all *O. dioica* CDK1 paralogs. *O. dioica* CDK2, the only CDK in this species with a conserved PSTAIRE, was dispensable for embryonic divisions, recalling the situation in plants, where the CDK1 ortholog, CDKA, which has the canonical PSTAIRE, is dispensable for the cell cycle, whereas CDKB, deviating in the PSTAIRE, has essential functions in the absence of CDKA (Nowack et al., 2012). Strikingly, the modified PSTAIRE of the *O. dioica* CDK1d paralog (PPTSLRE) shows convergence over great evolutionary distance with plant CDKB sequences (P[P/S]T [A/T]LRE), and in both *O. dioica*, and plants, these variants exhibit increased specialization to M-phase (Joubes et al., 2000; Nowack et al., 2012). The suite of naturally evolved *O. dioica*, CDK1:Cyclin B complexes, with critical residue substitutions in their activation segments, ATP binding sites, CDK1-Cyclin B interaction interfaces, and Cyclin B-substrate interaction elements, provide a fertile foundation for structural studies of how these changes elicit enhanced kinase selection for subsets of G2-M, CDK1 cell cycle substrates.

MATERIALS AND METHODS

Animal Culture and Collection

O. dioica were maintained in culture at 15°C (Bouquet et al., 2009). Day 4–6 animals were placed in filtered seawater, removed from their houses and anesthetized in cold ethyl 3-aminobenzoate methanesulfonate salt (MS-222, 0.125 mg/ml; Sigma) before collection.

In Vitro Fertilization and Collection of Synchronously Dividing Zygotes

Sperm solutions were prepared by transferring 5 mature males to a petri dish containing 10 ml artificial seawater, on ice, and sperm quality was assessed using a Nikon Eclipse E400 microscope. Mature females were transferred to artificial sea water in 24-well plates coated with 0.9% agarose, artificial sea water was changed every hour. Oocytes were fertilized with 400 µl sperm solution and fertilized oocytes were washed in 8 ml artificial sea water within 50 s. Synchronicity of fertilization was verified by following polar body exclusion and early cleavages.

Phylogenetic Analyses

A search of larvacean CDK1, CDK2 and Cyclin B proteins was performed using TBLASTN against genomes and transcriptomes of *Oikopleura albicans*, *O. longicauda*, *O. vanhoeffeni* and *Fritillaria borealis*. *O. dioica* CDK1, CDK2 and Cyclin Bc were used as queries with E-value cutoff set to 1e-005. *Ciona intestinalis* and *Branchiostoma floridae* proteins were obtained from the JGI Genome Portal (<https://genome.jgi.doe.gov/mycosm/home>). For identified targets, amino acid sequences of the N-terminal cyclin box or the kinase domain of CDK1/2 were aligned (clustalX). Alignments were manually edited (Bioedit), and secondary structure analysis (psipred) was used to guide alignments. Phylogenetic relationships were inferred using maximum likelihood (ML) using MEGA7 (Kumar et al., 2016), with amino acid sequence alignment based on Jones-Taylor-Thornton (Jones et al., 1992). Estimates of the gamma-shape parameter and proportion of invariant sites were then used to obtain the 500 bootstrap replicates.

Yeast Complementation

We used a W303a-background yeast wild-type strain SCU893 (*MATa ura3 ade2-1 trp1-1 leu2-3112 his3-11 bar1:hisG*) and its derivative SCU112 (*cdc28-4*). To complement a *cdc28* mutation of *S. cerevisiae*, the open reading frames of the *O. dioica* CDK1 paralogs and CDK2 cDNAs were cloned in pCR™4-TOPO® TA Vector (ThermoFisher). cDNA fragments were isolated by digestion with *EcoRI* and *NotI* and ligated into the yeast pYES2 expression vector (Invitrogen) downstream of the inducible GAL1 promoter. The resulting CDK1 paralog plasmids were individually transformed by the lithium acetate method (Ito et al., 1984) into the *S. cerevisiae* *cdc28-4* strain. As a control, *cdc28-4* was transformed with the empty pYES2 vector. The transformants were grown for 4 days at 25°C, and the resulting colonies were cultivated overnight at 25°C in CM-ura

medium containing glucose as a carbon source. The cells were pelleted, washed, resuspended in CM-ura medium containing 2% glycerol, and grown further at 25°C. After 4 h, the cells were pelleted and resuspended in CM-ura medium containing either glucose (2%), or galactose (2%)–raffinose (1%) as carbon source, and grown at 25°C, or the restrictive 36°C, respectively.

Antibodies

Rabbit polyclonal affinity-purified anti-Cyclin Ba/b (acetyl-NRDLNIQESGPVKAVVNAC-amide; acetyl-CLEFLRRFSRVAEETIDPKEY-amide), anti-CDK1b (acetyl-CPDFTKPTSLNVNTSLNEMDM-amide), anti-CDK1c (acetyl-MRKRNRIDRPPTQDLNNYC–amide), anti-CDK1d (acetyl-MIKAKSGTQDLSNYKRC-amide), and anti-lamin1 (acetyl-QSPISLPLPSGSTC-amide) were from 21st Century Biochemicals (Marlboro, MA). Other antibodies: anti-PSTAIR (Abcam, ab10345), anti-ATPB (Abcam, ab37922), anti-histone 3 (Abcam, ab10799), anti-H3-S28 (Abcam, ab10543), anti-GFP (AMS biotechnology, M30939-2). Secondary antibodies for immunofluorescence: goat anti-rabbit IgG (H+L) Alexa Fluor 568 (ThermoFisher, A-11011); and for western blots: goat anti-rabbit IgG (H+L) superclonal™ secondary antibody, HRP (ThermoFisher, A27033), Peroxidase-AffiniPure Goat Anti-Mouse IgG (H+L) (Jackson ImmunoResearch, 115-035-003).

Quantitative Reverse Transcription-PCR, Immunofluorescence and Western Blots

D3, D4, D5 males, D5 females, D6 males and D6 females were collected individually and snap frozen in liquid nitrogen. 50 Oocytes were collected from each ovary and were either snap frozen in liquid nitrogen or fertilized, with zygotes that were generated subsequently snap frozen. Total RNA was extracted from whole animals (D3, D4, D5, D6), oocytes and zygotes using Trizol (Life Technologies, Gaithersburg, MD, United States) and treated with RNase-free DNase (Roche, Indianapolis, IN, United States) according to manufacturer's instructions. For qRT-PCR, 1 µg of purified total RNA was subjected to RT using M-MLV reverse transcriptase (Invitrogen). Oligo (dT) was used as primer for cDNA synthesis. The quantitative polymerase chain reaction (qPCR) (CFX-96; Bio-Rad) was performed using cDNA templates synthesized from an equivalent of 5 ng total RNA, 10 µl of qPCR 2 Master Mix (Bio Rad), and 500 nM primers in a total volume of 20 µl. After initial denaturation for 5 min at 95°C, 45 cycles of 95°C for 15 s, 60°C for 20 s, and 72°C for 20 s were conducted, with a final extension for 5 min at 72°C. RT-negative controls were run to 45 cycles. RPL23 and EF-1β mRNA levels served as normalization controls in all qRT-PCRs. For RNAi experiments, target mRNA levels were normalized to control zygotes. Primer pair specificities were confirmed by melting curve evaluation, cloning, and sequencing of amplicons. In these experiments, mean values normalized to EF-1β control transcripts are presented and assessed by one-sided unpaired Student's t-test for equal variances, or, one-sided unpaired, Welch's t-test for unequal variances. Effect size was calculated as Cohen's $d = 2t/\text{SQRT}(df)$. Immunofluorescence and Western blots were performed as previously (Campsteijn et al., 2012). Quantification of bands was performed using ImageLab software (Bio-Rad, Hercules, CA).

Microinjection

Gonad microinjections were performed as previously (Ovrebo et al., 2015). Injection solutions were prepared by mixing double stranded RNA (dsRNA) in RNase free PBS at a final concentration of 300 ng/ μ l. Anesthetized day 4 or day 5 animals in filtered seawater were transferred to Petri dishes coated with 2% agarose. Gonads were injected with 1–2 nl dsRNA solution on a Nikon Eclipse TE2000-S inverted microscope equipped with Narishige micromanipulators and transjector 5246 micro injector (Eppendorf). Injected day 4/5 animals were transferred to watch glasses containing filtered seawater for recovery and then transferred to 6 L beakers for subsequent culture. Animals were cultured until spawning for *in vitro* fertilization (IVF) and immunofluorescence. Oocytes spawned from females where ovaries had been injected with dsRNA against target genes or from wild-type non-injected females (control) were transferred to 24-well plates coated with 0.9% agarose containing fresh artificial seawater (Red Sea) for 1 h. Samples of 50 oocytes spawned from each female (3 females per treatment group, except **Figure 5A**, $n1 = 2$) were used for qRT-PCR. Aliquots of 50 oocytes were also used for western blots. Remaining oocytes were fertilized and developmental defects arising from various treatments were assessed by unpaired Student's t-test for equal variances, or, unpaired, Welch's t-test for unequal variances. Effect size was calculated as Cohen's $d = 2t/\text{SQRT}(df)$.

In Vitro CDK1 Kinase Activities

CDK1 kinase activities were determined as previously (Feng and Thompson 2018). Equal numbers of oocytes were snap frozen and thawed twice. Cyclin Ba/b immunoprecipitates, purified his-Cyclin Ba-GST OdCDK1d complexes were aliquoted, kept at 80°C and thawed before use. Samples were mixed with biotinylated MV peptide and 1 mM ATP incubated at 30°C for 30 min. After stopping the phosphorylation reaction, ELISA was performed using anti-phospho MV peptide antibody (MESACUP) and the CDK1 Kinase Assay Kit (MBL). Finally, POD-conjugated streptavidin was used to detect phosphorylated MV peptide and color development measured at 492 nm. Differences in CDK1 kinase activities from different knockdown treatments were assessed by the Student's T-test. H1 kinase assays were performed as previously (Levasseur and McDougall 2000). After thawing snap frozen oocyte samples on ice, 2 μ l of 6 \times kinase reaction mixture (pH 7.2) containing histone H1 (Sigma type III from calf thymus), 0.6 mM ATP, 0.5 mCi/ml [³²P]ATP, and 60 μ M cAMP-dependent protein kinase inhibitor was added to 10 μ l of oocyte sample. The reaction was started by transfer to a 30°C heat block for 30 min and stopped by adding 5 \times Laemmli buffer. The samples were then heated to 80°C for 10 min and resolved on 15% polyacrylamide gels. Gels were placed in a Phosphorimager (Fujix; 1500 Bas Reader) and incorporation of [³²P] was quantified.

Capped mRNA and dsRNA Synthesis

O. dioica CDK1-eGFP fusion-constructs including endogenous 3'UTRs were linearized using *Xma*I (odCDK1a and d), *Afe*I (odCDK1e), or *Xba*I (H2B-eGFP) and purified by phenol-chloroform extraction followed by ethanol precipitation. Capped mRNAs were synthesized from these templates using mMessage mMachine (Ambion) followed by poly(A) tailing

(Ambion) according to the manufacturer's protocol and purified by Lithium chloride precipitation. Capped mRNA solutions at 1 μ g/ μ l were injected to oocytes. After exposure to wild-type sperm, tadpoles were fixed for immunostaining. For dsRNA synthesis, 300 bp fragments in the coding region of target sequences were amplified by PCR using gene-specific primers with T7 overhangs and purified by phenol-chloroform extraction. Sense and antisense RNA were synthesized in a single reaction following the recommended protocol using T7 RiboMAX™ Express RNAi system (Promega).

DATA AVAILABILITY STATEMENT

Publicly available datasets were analyzed in this study. This data can be found here: *Oikopleura dioica* genome and transcriptome are available at <http://www.genoscope.cns.fr>, <http://oikoarrays.biology.uiowa.edu/Oiko/> and transcription start site CAGE data at the NCBI Gene Expression Omnibus <https://www.ncbi.nlm.nih.gov/geo/> under accession number GSE78794. The *Fritillaria borealis* genome is available at GenBank <https://www.ncbi.nlm.nih.gov/genbank/>: SDII00000000 and other *Oikopleura* species genomes at GenBank SCLD01000000 to SCLH01000000.

AUTHOR CONTRIBUTIONS

XM and ET conceived and designed the experiments. XM performed experiments and XM and ET analyzed the data. JØ performed CDK1-GFP cmRNA injection and immunostaining. XM and ET wrote the manuscript. All authors approved the manuscript.

FUNDING

This work was supported by grants 183690/S10 NFR-FUGE and 133335/V40 from the Norwegian Research Council (ET).

ACKNOWLEDGMENTS

We thank Haiyang Feng, for helpful discussion and A. Aasjord and K. N. Nøkling for providing animals from the *Oikopleura* culture facility. Yeast strains were provided by Jorrit Enserink, University of Oslo. We thank the Chourrout S1 group at the Sars Centre for early access to sequence data from hermaphroditic appendicularian species.

SUPPLEMENTARY MATERIAL

The Supplementary Material for this article can be found online at: <https://www.frontiersin.org/articles/10.3389/fcell.2021.770939/full#supplementary-material>

REFERENCES

- Ahn, S.-H., Tobe, B. T., Gerald, J. N. F., Anderson, S. L., Acurio, A., and Kron, S. J. (2001). Enhanced Cell Polarity in Mutants of the Budding Yeast Cyclin-dependent Kinase Cdc28p. *MBoC* 12, 3589–3600. doi:10.1091/mbc.12.11.3589
- Arooz, T., Yam, C. H., Siu, W. Y., Lau, A., Li, K. K. W., and Poon, R. Y. C. (2000). On the Concentrations of Cyclins and Cyclin-dependent Kinases in Extracts of Cultured Human Cells. *Biochemistry* 39, 9494–9501. doi:10.1021/bi0009643
- Bachtrog, D., Jensen, J. D., and Zhang, Z. (2009). Accelerated Adaptive Evolution on a Newly Formed X Chromosome. *Plos Biol.* 7, e28e1000082. doi:10.1371/journal.pbio.1000082
- Bao, Z. Q., Jacobsen, D. M., and Young, M. A. (2011). Briefly Bound to Activate: Transient Binding of a Second Catalytic Magnesium Activates the Structure and Dynamics of Cdk2 Kinase for Catalysis. *Structure* 19, 675–690. doi:10.1016/j.str.2011.02.016
- Bentley, A. M., Normand, G., Hoyt, J., and King, R. W. (2007). Distinct Sequence Elements of Cyclin B1 Promote Localization to Chromatin, Centrosomes, and Kinetochores during Mitosis. *MBoC* 18, 4847–4858. doi:10.1091/mbc.E06-06-0539
- Bouquet, J.-M., Spriet, E., Troedsson, C., Ottera, H., Chourrout, D., and Thompson, E. M. (2009). Culture Optimization for the Emergent Zooplanktonic Model Organism *Oikopleura dioica*. *J. Plankton Res.* 31, 359–370. doi:10.1093/plankt/fbn132
- Brown, N. R., Korolchuk, S., Martin, M. P., Stanley, W. A., Moukhametzianov, R., Noble, M. E. M., et al. (2015). Cdk1 Structures Reveal Conserved and Unique Features of the Essential Cell Cycle Cdk. *Nat. Commun.* 6, 6769. doi:10.1038/ncomms7769
- Brown, N. R., Noble, M. E. M., Endicott, J. A., and Johnson, L. N. (1999). The Structural Basis for Specificity of Substrate and Recruitment Peptides for Cyclin-dependent Kinases. *Nat. Cell Biol.* 1, 438–443. doi:10.1038/15674
- Campsteijn, C., Ovrebo, J. I., Karlsen, B. O., and Thompson, E. M. (2012). Expansion of Cyclin D and Cdk1 Paralogs in *Oikopleura dioica*, a Chordate Employing Diverse Cell Cycle Variants. *Mol. Biol. Evol.* 29, 487–502. doi:10.1093/molbev/msr136
- Chen, C., Ha, B. H., Thévenin, A. F., Lou, H. J., Zhang, R., Yip, K. Y., et al. (2014). Identification of a Major Determinant for Serine-Threonine Kinase Phosphoacceptor Specificity. *Mol. Cell* 53, 140–147. doi:10.1016/j.molcel.2013.11.013
- Connallon, T., and Clark, A. G. (2011). The Resolution of Sexual Antagonism by Gene Duplication. *Genetics* 187, 919–937. doi:10.1534/genetics.110.123729
- Creixell, P., Palmeri, A., Miller, C. J., Lou, H. J., Santini, C. C., Nielsen, M., et al. (2015). Unmasking Determinants of Specificity in the Human Kinome. *Cell* 163, 187–201. doi:10.1016/j.cell.2015.08.057
- Danks, G. B., Navratilova, P., Lenhard, B., and Thompson, E. M. (2018). Distinct Core Promoter Codes Drive Transcription Initiation at Key Developmental Transitions in a marine Chordate. *BMC Genomics* 19, 164. doi:10.1186/s12864-018-4504-5
- Danks, G. B., Raasholm, M., Campsteijn, C., Long, A. M., Manak, J. R., Lenhard, B., et al. (2015). Trans-splicing and Operons in Metazoans: Translational Control in Maternally Regulated Development and Recovery from Growth Arrest. *Mol. Biol. Evol.* 32, 585–599. doi:10.1093/molbev/msu336
- Danks, G., Campsteijn, C., Parida, M., Butcher, S., Doddapaneni, H., Fu, B., et al. (2013). OikoBase: a Genomics and Developmental Transcriptomics Resource for the Urochordate *Oikopleura dioica*. *Nucleic Acids Res.* 41, D845–D853. doi:10.1093/nar/gks1159
- Deibel, D., and Lowen, B. (2012). A Review of the Life Cycles and Life-History Adaptations of Pelagic Tunicates to Environmental Conditions. *ICES J. Mar. Sci.* 69, 358–369. doi:10.1093/icesjms/fsr159
- Des Marais, D. L., and Rausher, M. D. (2008). Escape from Adaptive Conflict after Duplication in an Anthocyanin Pathway Gene. *Nature* 454, 762–765. doi:10.1038/nature07092
- Echalier, A., Cot, E., Camasses, A., Hodimont, E., Hoh, F., Jay, P., et al. (2012). An Integrated Chemical Biology Approach Provides Insight into Cdk2 Functional Redundancy and Inhibitor Sensitivity. *Chem. Biol.* 19, 1028–1040. doi:10.1016/j.chembiol.2012.06.015
- Edgar, B. A., and Orr-Weaver, T. L. (2001). Endoreplication Cell Cycles. *Cell* 105, 297–306. doi:10.1016/S0092-8674(01)00334-8
- Edgar, B. A., Sprenger, F., Duronio, R. J., Leopold, P., and O'Farrell, P. H. (1994). Distinct Molecular Mechanism Regulate Cell Cycle Timing at Successive Stages of *Drosophila* Embryogenesis. *Genes Dev.* 8, 440–452. doi:10.1101/gad.8.4.440
- Farrell, J. A., and O'Farrell, P. H. (2014). From Egg to Gastrula: How the Cell Cycle Is Remodeled during the *Drosophila* Mid-blastula Transition. *Annu. Rev. Genet.* 48, 269–294. doi:10.1146/annurev-genet-111212-133531
- Farrell, J. A., Shermoen, A. W., Yuan, K., and O'Farrell, P. H. (2012). Embryonic Onset of Late Replication Requires Cdc25 Down-Regulation. *Genes Dev.* 26, 714–725. doi:10.1101/gad.186429.111
- Feng, H., and Thompson, E. M. (2018). Specialization of Cdk1 and Cyclin B Paralog Functions in a Coenocystic Mode of Oogenic Meiosis. *Cell Cycle* 17, 1425–1444. doi:10.1080/15384101.2018.1486167
- Fleig, U. N., Gould, K. L., and Nurse, P. (1992). A Dominant Negative Allele of P34cdc2 Shows Altered Phosphoamino Acid Content and Sequesters P56cdc13 Cyclin. *Mol. Cell Biol.* 12, 2295–2301. doi:10.1128/mcb.12.5.2295-2301.1992
- Ganot, P., Bouquet, J.-M., Kallestø, T., and Thompson, E. M. (2007). The *Oikopleura* Coenocyst, a Unique Chordate Germ Cell Permitting Rapid, Extensive Modulation of Oocyte Production. *Develop. Biol.* 302, 591–600. doi:10.1016/j.ydbio.2006.10.021
- Ganot, P., Bouquet, J.-M., and Thompson, E. M. (2006). Comparative Organization of Follicle, Accessory Cells and Spawning Anlagen in Dynamic Semelparous Clutch Manipulators, the Urochordate Oikopleuridae. *Biol. Cell* 98, 389–401. doi:10.1042/Bc20060005
- Ganot, P., and Thompson, E. M. (2002). Patterning through Differential Endoreduplication in Epithelial Organogenesis of the Chordate, *Oikopleura dioica*. *Develop. Biol.* 252, 59–71. doi:10.1006/dbio.2002.0834
- Goda, T., Funakoshi, M., Suhara, H., Nishimoto, T., and Kobayashi, H. (2001). The N-Terminal Helix of *Xenopus* Cyclins A and B Contributes to Binding Specificity of the Cyclin-Cdk Complex. *J. Biol. Chem.* 276, 15415–15422. doi:10.1074/jbc.M011101200
- Holt, L. J., Tuch, B. B., Villén, J., Johnson, A. D., Gygi, S. P., and Morgan, D. O. (2009). Global Analysis of Cdk1 Substrate Phosphorylation Sites Provides Insights into Evolution. *Science* 325, 1682–1686. doi:10.1126/science.1172867
- Huang, H., Zhao, R., Dickson, B. M., Skeel, R. D., and Post, C. B. (2012). α C Helix as a Switch in the Conformational Transition of Src/CDK-like Kinase Domains. *J. Phys. Chem. B* 116, 4465–4475. doi:10.1021/jp301628r
- Huang, J., and Ruff, J. W. (1999). The Disappearance of Cyclin B at the End of Mitosis Is Regulated Spatially in *Drosophila* Cells. *EMBO J.* 15, 2184–2195. doi:10.1093/emboj/18.8.2184
- Ito, H., Murata, K., and Kimura, A. (1984). Transformation of Intact Yeast Cells Treated with Alkali Cations or Thiol Compounds. *Agric. Biol. Chem.* 48, 341–347. doi:10.1080/00021369.1984.10866161
- Jeffrey, P. D., Russo, A. A., Polyak, K., Gibbs, E., Hurwitz, J., Massagué, J., et al. (1995). Mechanism of Cdk Activation Revealed by the Structure of a Cyclin-Cdk2 Complex. *Nature* 376, 313–320. doi:10.1038/376313a0
- Jones, D. T., Taylor, W. R., and Thornton, J. M. (1992). The Rapid Generation of Mutation Data Matrices from Protein Sequences. *Bioinformatics* 8, 275–282. doi:10.1093/bioinformatics/8.3.275
- Joubès, J., Chevalier, C., Dudits, D., Heberle-Bors, E., Inzé, D., Umeda, M., et al. (2000). Cdk-related Protein Kinases in Plants. *Plant Mol. Biol.* 43, 607–620. doi:10.1023/a:1006470301554
- Katsuno, Y., Suzuki, A., Sugimura, K., Okumura, K., Zineldeen, D. H., Shimada, M., et al. (2009). Cyclin A-Cdk1 Regulates the Origin Firing Program in Mammalian Cells. *Proc. Natl. Acad. Sci.* 106, 3184–3189. doi:10.1073/pnas.0809350106
- Kõivomägi, M., Valk, E., Venta, R., Iofik, A., Lepiku, M., Morgan, D. O., et al. (2011). Dynamics of Cdk1 Substrate Specificity during the Cell Cycle. *Mol. Cell* 42, 610–623. doi:10.1016/j.molcel.2011.05.016
- Kumar, S., Stecher, G., and Tamura, K. (2016). MEGA7: Molecular Evolutionary Genetics Analysis Version 7.0 for Bigger Datasets. *Mol. Biol. Evol.* 33, 1870–1874. doi:10.1093/molbev/msw054
- Larochelle, S., Merrick, K. A., Terret, M.-E., Wohlbold, L., Barboza, N. M., Zhang, C., et al. (2007). Requirements for Cdk7 in the Assembly of Cdk1/cyclin B and Activation of Cdk2 Revealed by Chemical Genetics in Human Cells. *Mol. Cell* 25, 839–850. doi:10.1016/j.molcel.2007.02.003
- Lemmens, B., Hegarat, N., Akopyan, K., Sala-Gaston, J., Bartek, J., Hohegger, H., et al. (2018). DNA Replication Determines Timing of Mitosis by Restricting

- CDK1 and PLK1 Activation. *Mol. Cell* 71, 117–128. doi:10.1016/j.molcel.2018.05.026
- Levasseur, M. D., Thomas, C., Davies, O. R., Higgins, J. M. G., and Madgwick, S. (2019). Aneuploidy in Oocytes Is Prevented by Sustained Cdk1 Activity through Degron Masking in Cyclin B1. *Development* 48, 672–684. doi:10.1016/j.devcel.2019.01.008
- Levasseur, M., Dumollard, R., Chambon, J.-P., Hebras, C., Sinclair, M., Whitaker, M., et al. (2013). Release from Meiotic Arrest in Ascidian Eggs Requires the Activity of Two Phosphatases but Not Camkii. *Development* 140, 4583–4593. doi:10.1242/dev.096578
- Levasseur, M., and McDougall, A. (2000). Sperm-induced Calcium Oscillations at Fertilisation in Ascidians Are Controlled by Cyclin B1-dependent Kinase Activity. *Development* 127, 631–641. doi:10.1242/dev.127.3.631
- Levine, K., Kiang, L., Jacobson, M. D., Fisher, R. P., and Cross, F. R. (1999). Directed Evolution to Bypass Cyclin Requirements for the Cdc28p Cyclin-dependent Kinase. *Mol. Cell* 4, 353–363. doi:10.1016/S1097-2765(00)80337-8
- Lobón, C., Acuña, J., López-Álvarez, M., and Capitano, F. (2011). Heritability of Morphological and Life History Traits in a Pelagic Tunicate. *Mar. Ecol. Prog. Ser.* 422, 145–154. doi:10.3354/meps08923
- Macneill, S. A., and Nurse, P. (1993). Mutational Analysis of the Fission Yeast P34cdc2 Protein Kinase Gene. *Mol. Gen. Genet.* 236, 415–426. doi:10.1007/BF00277142
- Nakanishi, M., Katsuno, Y., Niida, H., Murakami, H., and Shimada, M. (2010). Chk1-cyclin A/Cdk1 axis Regulates Origin Firing Programs in Mammals. *Chromosome Res.* 18, 103–113. doi:10.1007/s10577-009-9086-2
- Naville, M., Henriot, S., Warren, I., Sumic, S., Reeve, M., Volff, J.-N., et al. (2019). Massive Changes of Genome Size Driven by Expansions of Non-autonomous Transposable Elements. *Curr. Biol.* 29, 1161–1168. doi:10.1016/j.cub.2019.01.080
- Nolen, B., Taylor, S., and Ghosh, G. (2004). Regulation of Protein Kinases. *Mol. Cell* 15, 661–675. doi:10.1016/j.molcel.2004.08.024
- Nowack, M. K., Harashima, H., Dissmeyer, N., Zhao, X. A., Bouyer, D., Weimer, A. K., et al. (2012). Genetic Framework of Cyclin-dependent Kinase Function in Arabidopsis. *Development* 141, 1030–1040. doi:10.1016/j.devcel.2012.02.015
- Okano-Uchida, T., Sekiai, T., Lee, K.-s., Okumura, E., Tachibana, K., and Kishimoto, T. (1998). In Vivo Regulation of Cyclin A/Cdc2 and Cyclin B/Cdc2 through Meiotic and Early Cleavage Cycles in Starfish. *Development* 125, 39–53. doi:10.1006/dbio.1998.8881
- Örd, M., and Loog, M. (2019). How the Cell Cycle Clock Ticks. *MBio* 30, 169–172. doi:10.1091/mbc.E18-05-0272
- Örd, M., Möll, K., Agerova, A., Kivi, R., Faustova, I., Venta, R., et al. (2019a). Multisite Phosphorylation Code of Cdk. *Nat. Struct. Mol. Biol.* 26, 649–658. doi:10.1038/s41594-019-0256-4
- Örd, M., Venta, R., Möll, K., Valk, E., and Loog, M. (2019b). Cyclin-specific Docking Mechanisms Reveal the Complexity of M-Cdk Function in the Cell Cycle. *Mol. Cell* 75, 76–89. doi:10.1016/j.molcel.2019.04.026
- Øvrebo, J. I., Campsteijn, C., Kourtesis, I., Hausen, H., Raasholm, M., and Thompson, E. M. (2015). Functional Specialization of Chordate Cdk1 Paralogs during Oogenic Meiosis. *Cell Cycle* 14, 880–893. doi:10.1080/15384101.2015.1006000
- Rogozin, I. B., Belinky, F., Pavlenko, V., Shabalina, S. A., Kristensen, D. M., and Koonin, E. V. (2016). Evolutionary Switches between Two Serine Codon Sets Are Driven by Selection. *Proc. Natl. Acad. Sci. USA* 113, 13109–13113. doi:10.1073/pnas.1615832113
- Santamaría, D., Barrière, C., Cerqueira, A., Hunt, S., Tardy, C., Newton, K., et al. (2007). Cdk1 Is Sufficient to Drive the Mammalian Cell Cycle. *Nature* 448, 811–815. doi:10.1038/nature06046
- Schaffner, S. F. (2004). The X Chromosome in Population Genetics. *Nat. Rev. Genet.* 5, 43–51. doi:10.1038/nrg1247
- Seller, C. A., and O'Farrell, P. H. (2018). Rfl1 Prolongs the Embryonic S Phase at the *Drosophila* Mid-blastula Transition. *Plos Biol.* 16, e2005687. doi:10.1371/journal.pbio.2005687
- Sonnhammer, E. L. L., and Koonin, E. V. (2002). Orthology, Paralogy and Proposed Classification for Paralog Subtypes. *Trends Genet.* 18, 619–620. doi:10.1016/S0168-9525(02)02793-2
- Staver, J. M., and Strathmann, R. R. (2002). Evolution of Fast Development of Planktonic Embryos to Early Swimming. *Biol. Bull.* 203, 58–69. doi:10.2307/1543458
- Strathmann, R. R., Staver, J. M., and Hoffman, J. R. (2002). Risk and the Evolution of Cell-Cycle Durations of Embryos. *Evolution* 56, 708–720. doi:10.1111/j.0014-3820.2002.tb01382.x
- Swaffer, M. P., Jones, A. W., Flynn, H. R., Snijders, A. P., and Nurse, P. (2016). Cdk Substrate Phosphorylation and Ordering the Cell Cycle. *Cell* 167, 1750–1761. doi:10.1016/j.cell.2016.11.034
- Szmyd, R., Niska-Blakie, J., Diril, M. K., Renck Nunes, P., Tzelepis, K., Lacroix, A., et al. (2019). Premature Activation of Cdk1 Leads to Mitotic Events in S Phase and Embryonic Lethality. *Oncogene* 38, 998–1018. doi:10.1038/s41388-018-0464-0
- Troedsson, C., Bouquet, J., Aksnes, D., and Thompson, E. (2002). Resource Allocation between Somatic Growth and Reproductive Output in the Pelagic Chordate *Oikopleura dioica* Allows Opportunistic Response to Nutritional Variation. *Mar. Ecol. Prog. Ser.* 243, 83–91. doi:10.3354/meps243083
- Tsai, T. Y.-C., Theriot, J. A., and Ferrell, J. E. (2014). Changes in Oscillatory Dynamics in the Cell Cycle of Early *Xenopus laevis* Embryos. *Plos Biol.* 12, e1001788. doi:10.1371/journal.pbio.1001788
- van der Voet, M., Lorson, M., Srinivasan, D. G., Bennett, K. L., and van den Heuvel, S. (2009). C. Elegans mitotic Cyclins Have Distinct as Well as Overlapping Functions in Chromosome Segregation. *Cell Cycle* 8, 4091–4102. doi:10.4161/cc.8.24.10171
- Vulpetti, A., and Bosotti, R. (2004). Sequence and Structural Analysis of Kinase ATP Pocket Residues. *Il Farmaco* 59, 759–765. doi:10.1016/j.farmac.2004.05.010
- Wood, D. J., Korolchuk, S., Tatum, N. J., Wang, L.-Z., Endicott, J. A., Noble, M. E. M., et al. (2019). Differences in the Conformational Energy Landscape of CDK1 and CDK2 Suggest a Mechanism for Achieving Selective CDK Inhibition. *Cel Chem. Biol.* 26, 121–130. doi:10.1016/j.chembiol.2018.10.015
- Yang, Z. (2007). Paml 4: Phylogenetic Analysis by Maximum Likelihood. *Mol. Biol. Evol.* 24, 1586–1591. doi:10.1093/molbev/msm088
- Yuan, K., Seller, C. A., Shermoen, A. W., and O'Farrell, P. H. (2016). Timing the *Drosophila* Mid-blastula Transition: A Cell Cycle-Centered View. *Trends Genet.* 32, 496–507. doi:10.1016/j.tig.2016.05.006
- Zhang, J., Rosenberg, H. F., and Nei, M. (1998). Positive Darwinian Selection after Gene Duplication in Primate Ribonuclease Genes. *Proc. Natl. Acad. Sci.* 95, 3708–3713. doi:10.1073/pnas.95.7.3708

Conflict of Interest: The authors declare that the research was conducted in the absence of any commercial or financial relationships that could be construed as a potential conflict of interest.

Publisher's Note: All claims expressed in this article are solely those of the authors and do not necessarily represent those of their affiliated organizations, or those of the publisher, the editors and the reviewers. Any product that may be evaluated in this article, or claim that may be made by its manufacturer, is not guaranteed or endorsed by the publisher.

Copyright © 2022 Ma, Øvrebo and Thompson. This is an open-access article distributed under the terms of the Creative Commons Attribution License (CC BY). The use, distribution or reproduction in other forums is permitted, provided the original author(s) and the copyright owner(s) are credited and that the original publication in this journal is cited, in accordance with accepted academic practice. No use, distribution or reproduction is permitted which does not comply with these terms.